

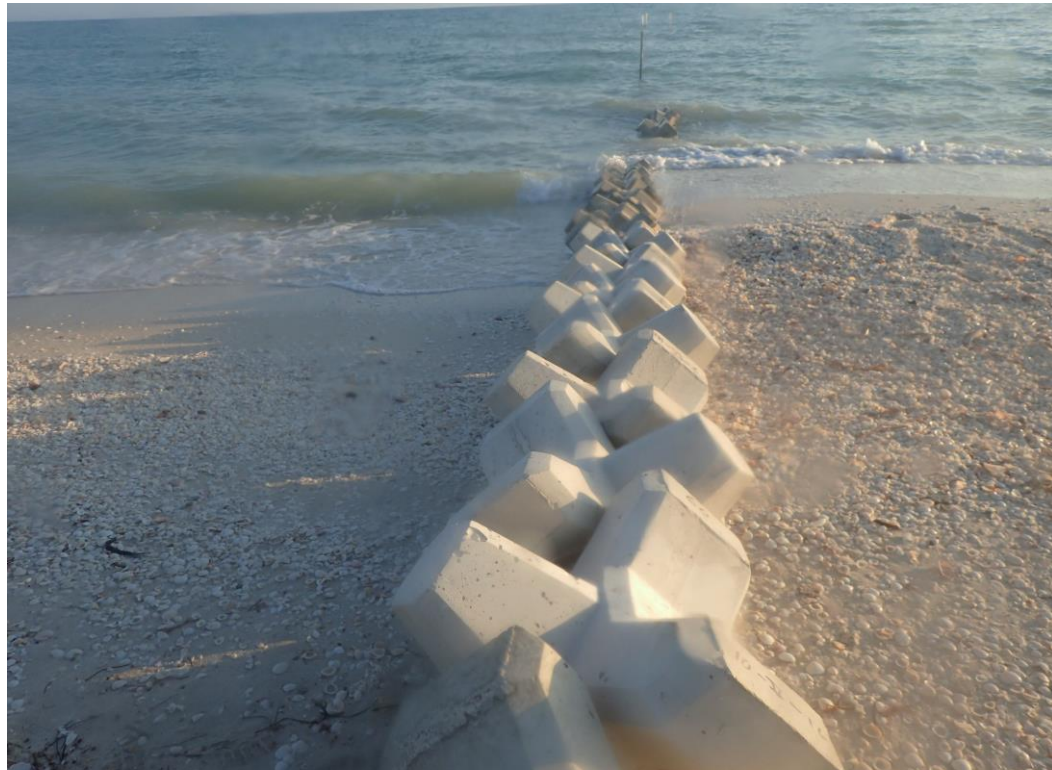
JULY 8, 2016

UNIVERSITY OF TWENTE.



LIPC
LABORATORIO DE INGENIERÍA
Y PROCESOS COSTEROS
 UNAM

**INSTITUTO
DE INGENIERÍA
UNAM**



The permeable groin used at the beach site in action (*photographed by author*).

ON THE ROLE OF A PERMEABLE GROIN IN BEACH MORPHODYNAMICS DURING SEA-BREEZE EVENTS

Supervisors:
Dr. Ir. P.C. Roos – University of Twente
Dr. A. Torres Freyermuth – II-UNAM

Anne Hofman
University of Twente |
Universidad Nacional
Autonóma de Mexico

On the role of a permeable groin in beach morphodynamics during sea-breeze events

Date: July 8th, 2016

Place: Sisal, Yucatán, Mexico

Author: A. (Anne) Hofman

UT Student number: s1356992

Version: Final version.

Institutions involved: Laboratorio de Ingeniería y Procesos Costeros (LIPC)
Instituto de Ingeniería,
Universidad Nacional Autónoma de México (UNAM)
Puerto de Abrigo S/N,
97355 Sisal, Yucatán
Mexico

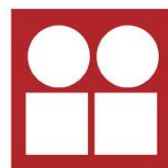
University of Twente
Faculty of Engineering Technology (CTW)
Department of Civil Engineering
Postbus 217
7500 AE Enschede

Supervisors: Dr. A. Torres-Freyermuth LIPC/II-UNAM
Dr. Ir. P.C. Roos University of Twente, WEM

UNIVERSITY OF TWENTE.



LIPC
LABORATORIO DE INGENIERÍA
Y PROCESOS COSTEROS
 UNAM



**INSTITUTO
DE INGENIERÍA
UNAM**

Summary

While not directly in the line of most hurricanes that strike the peninsula or head to the United States, the north coast of the Yucatán peninsula is vulnerable to various physical and socio-economic impacts due to strong winds and storms. Strong winds cause energetic waves to occur, despite the area being a low-energy wave area due to the wide and shallow continental shelf. Strong diurnal sea breezes drive sediment transport parallel to the coast, while ports and coastal structures induce large longshore transport gradients, hence beach erosion is obliquus in causing damage in coastal infrastructure along the coast. In order to solve local erosion problems, local measurements involving impermeable structures are often introduced as a coastal mitigation measure. However, these measurements often cause downdrift erosion problems due to the lessening of sediment budget transferred along the coast.

In order to create a solution for the downdrift effect of impermeable structures, a permeable structure was tested in Sisal, Yucatán during one sea-breeze event. Field observations were conducted to characterize natural wave conditions, wind climate, tidal climate and beach morphology. Testing was done using a 24h experiment, in which continuous monitoring of beach morphology ensured correlation with natural forcing conditions. Afterwards, beach recovery was monitored to get an impression regarding beach resilience. Results were compared to observations from a similar field experiment conducted with an impermeable groin.

During spring period, natural variability of the beach in Sisal was found to be tied to sea-breeze events. From interpretation of the longshore sediment transport formulas of Kamphuis and the USACE/CERC it was estimated that the rate of longshore sediment transport was influenced by local sea conditions. Volumetric change varied during the day, with beach profiles closely near the (semi)-permeable groin showing volumetric gain at the updrift side and erosion at the downdrift side. Shoreline change around the permeable groin resembled closely the typical pattern found at shoreline changes around an impermeable groin marked by volume gain on the updrift side and volume loss found on the downdrift side. The impact of the permeable groin on the beach over 24h is significantly less, expressed in the total volume gain of 18 m³ for the permeable groin and 60 m³ for the impermeable groin. Beach resilience was found to be very strong, with the beach being able to recover from the influence of the structure within 24 hours after removal of the permeable groin.

Due to the big similarity between the shoreline changes around impermeable and permeable groins, it was concluded that the impermeable groin used during the experiment did not possess a significant advantage over the use of an impermeable groin. Also, it was concluded that despite permeable groin not having a quantitative advantage over the permeable groin, it had a qualitative advantage, it being able to reduce downdrift erosion problems due to its permeability on short term. However, long term advantages/disadvantages could not properly be assessed and therefore, it was recommended that long-time effects of a permeable groin have to be inspected and that the different degrees of permeability should be tested.

Foreword

This thesis was conceived, researched and written during 11 weeks at the Universidad Nacional Autónoma de México, in the Laboratorio de Ingeniería y Procesos Costeros. During my time at the University here, I have met many new people, learned a lot of skills regarding the use of instruments, and gained a new impression of doing research on an academic level. The thesis report you are about to read is a result of 10 weeks of hard work.

During my stay at the LIPC, my goal was to obtain more affinity with practical research, most notably setting up and performing an experiment with the objective of describing a morphological phenomenon within a model context. My research theme was well suited to my goal, and I learnt a lot during the time I preformed my research at the LIPC.

Numerous people helped me over the course of my bachelor's thesis, and I am highly grateful for their assistance. First of all, I would like to thank Alec Torres-Freyermuth for being my supervisor here in Mexico. I always could rely on you if I needed any help, and you always attempted to challenge me by explaining me opportunities that were hidden in the data. Secondly, I would like to thank Pieter Roos for being my supervisor from the UT. I could e-mail you at any time with any question, and you would answer it straight and honestly and provide me with excellent feedback. Last of all, I would really like to thank Gabriela Medellín Mayoral for helping me getting familiar with all the equipment used before, during, and after the experiment. I could always walk into your office if I did not completely understand something, and you would always take your time with me explaining how things worked or how the data looked. Lastly, I would like to thank everybody from the faculty and students involved during the field experiment, most notably Gonzalo Martín Ruiz and José Lopez Gonzalez.

I hope to provide the reader of this report an insight into the world of beach morphology, and wish the reader a good time reading this report.

Anne Hofman,
Mexico, 8th of July 2016

Table of Contents

Summary	2
Foreword	3
Table of Figures	5
1. Introduction	6
1.1 Project framework.....	6
1.2 Background	6
1.3 Problem definition	8
1.4 Research aim and research questions	8
1.5 Reading guide	8
2. Study area	9
3. Theoretical background	11
3.1 Wind waves	11
3.2 Sediment transport due to wave action	12
3.3 Shoreline change due to divergence of longshore sediment flux	14
4. Methodology	16
4.1 Experiment setup and structure design	16
4.2 Measurements of conditions	18
4.3 Data reduction and correction	19
5. Results	22
5.1 Natural variability.....	22
5.2 Impact of a permeable groin during one sea-breeze event	26
5.3 Beach resilience after 24 hours	33
5.4 Shoreline change: impermeable versus permeable groin (1).....	34
5.5 Longshore transport rate	35
6. Discussion	37
6.1 Review of assumptions	37
6.2 Shoreline change: impermeable versus permeable groin (2).....	38
6.3 (Semi)-Permeable groin in erosion prevention	39
7. Conclusion and recommendations	40
7.1 Conclusion.....	40
7.2 Recommendations.....	41
8. References	42
Appendix A. Overview of used instruments.....	44

Table of Figures

Figure 1. Overview of Sisal within Yucatán, and an image of the beachfront at Sisal.....	6
Figure 2. Example of an impermeable groin on the beach of Progreso, Yucatán.....	7
Figure 3. View of the beachfront at the experimental site in Sisal.	9
Figure 4. Map of the Yucatan Shelf (Campeche Bank).....	10
Figure 5. An example of undertow	13
Figure 6. Visualization of longshore sediment transport.	13
Figure 7. Development of shoreline around an impermeable groin	15
Figure 8. Overview of experimental site in the Yucatán area.	16
Figure 9. Overview of field experiment site with position of instruments and the groin, and an overview of terminology used regarding the experimental site.....	16
Figure 10. Images of the groin setup with interlocking of the elements.	17
Figure 11. Axes setup for the instruments used.	19
Figure 12. Wind speed and wind direction measured during 10 days, from 10 to 20 May.....	22
Figure 13. (a) Significant wave height plotted versus wind speed and (b) current direction	23
Figure 14. (a) Intra-day variability of bed level in transect 10 and (b) the course of bed level profile of transect 10 over two days.	24
Figure 15. Shoreline position at an isobath of -0.3 m for the inter- and intra-day measurements on the updrift side of the groin.	25
Figure 16. Percentage of deviation of (a) accretion threshold of + 0.09 m bed level difference and (b) erosion threshold of - 0.09 m bed level difference for the intra-day measurements.	25
Figure 17. (a) Wind speed and wind direction and (b) predominant wind directions during the experiment period.	26
Figure 18. Significant wave height during the experiment period obtained with the 1/3 rd highest wave method (blue) and the 4 times standard deviation method (red).	26
Figure 19. Significant wave height (a) versus cross-shore (b) and alongshore (c) velocity.....	27
Figure 20. Plots of (a) significant wave height, (b) current velocity, (c) current direction and (d) predicted tide at Progreso (CICESE) versus measured water levels by the ADV.....	28
Figure 21. Bed level change over cross-shore distance in time (a,c) and evolution of bed level (b,d) for the transects 10 (directly updrift) and 12 (directly downdrift of the groin).....	29
Figure 22. Percentage of deviation of the (a) accretion threshold of + 0.09 m bed level difference and (b) erosion threshold of - 0.09 m bed level difference for the measurements during the experiment period.	30
Figure 23. (a) Shoreline change and (b) shoreline change relative to the first measurement at an isobath of -0.3 m	31
Figure 24. Contourplot of shoreline positon at (a) the start of measurements and (b) after 24 hours of structural influence.	31
Figure 25. Volumetric gain over time.	32
Figure 26. Shoreline change relative to the first measurement (M1) for the postmeasurements.	33
Figure 27. Percentage of deviation of the (a) accretion threshold of + 0.09 m bed level difference and (b) erosion threshold of - 0.09 m bed level difference for beach resilience.	33
Figure 28. Shoreline change for an (a) impermeable and (b) permeable groin.....	34
Figure 29. Overview of RTK position and setup.	44
Figure 30. RTK equipment used to measure transect change.	45
Figure 31. Vector head and axis (a), and components of the Nortek Vector (b).	46
Figure 32. An RD Instruments ADCP.....	47

1. Introduction

In this chapter, a general introduction is given to the reader. Section 1.1 describes the scientific framework of the research and section 1.2 gives background information for the project.

1.1 Project framework

The National Autonomous University of Mexico (UNAM) is the biggest university in Mexico with satellite campuses along the country. In the state of Yucatán, a satellite campus is located in Sisal along the northern shore of the Yucatán peninsula. The campus in Sisal hosts the Laboratorio y Ingeniería de Procesos Costeros (LIPC). The objective of LANRESC is to investigate the coastal processes and their associated resilience to different types of perturbations (i.e. natural or anthropogenic) including extreme events, coastal development and climate change.

1.2 Background

As population increases along coastal areas, pressure on ecological systems increases, resulting in human intervention in these areas. This is particularly important in context of climate change in low lying areas such as the Yucatán peninsula. The Yucatán peninsula is a region in southeastern Mexico, which separates the Gulf of Mexico and the Caribbean Sea. It is one of the richest environmental systems on the planet, but poor management and human intervention have resulted in a fragile ecosystem without a proper monitoring and management system, in turn resulting in increased risk and vulnerability to the coast (Appendini et al., 2012).

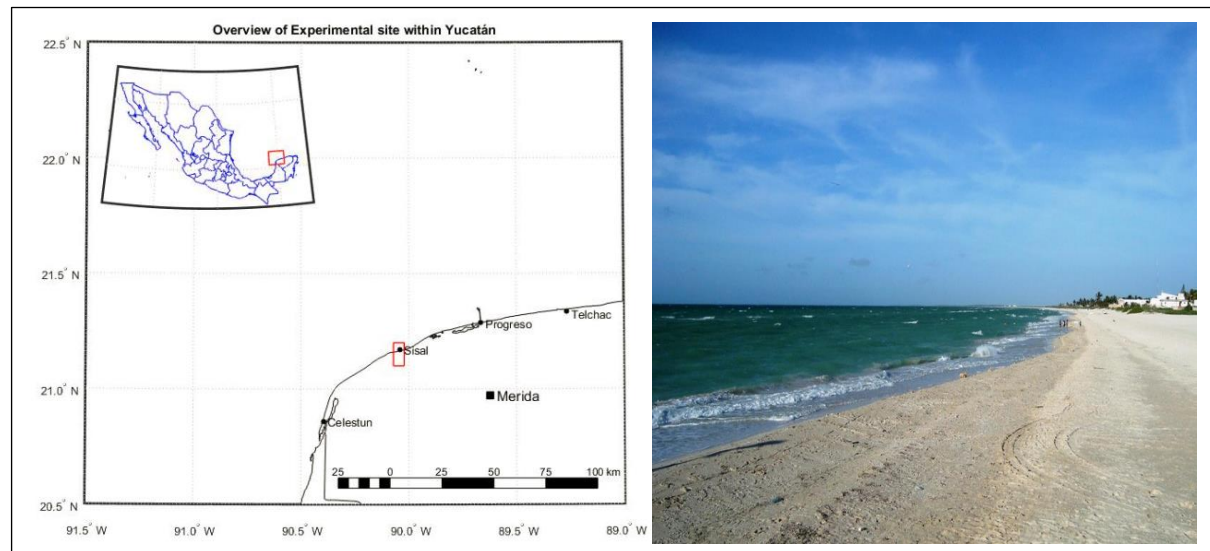


Figure 1. Overview of Sisal within Yucatán, and an image of the beachfront at Sisal (*photographed by author*).

While not directly in the line of most hurricanes that strike the peninsula or head to the United States, the north coast of the Yucatán peninsula, visible in figure 1, is vulnerable to various physical and socio-economic impacts due to storms (Meyer-Arendt, 1991). The geographic orientation of the coast makes the coast vulnerable to waves and storm activity heading from the Gulf of Mexico to the Yucatán peninsula, causing high pressure systems that send winds predominantly from the northeast (*Nortes*) towards the peninsula. On the other hand, strong sea breezes dominate mean wave climate, driving littoral transport along the coast, causing large longshore transport gradients and beach erosion along the coast. Due to the importance of longshore sediment transport, the Yucatán coast is very sensitive to the introduction of coastal structures.

A high rate of urbanization along the Yucatán coast, related to the development of economic activities and tourism along the coast, causes a significant alteration of the coastline. While

economic and touristic activities stir the construction of ports, harbors and vacation homes, the historical shoreline is significantly altered and natural transport processes of transgression and regression are interrupted (Meyer-Arendt, 2001). Structures such as harbors and ports have significant effect on the longshore sediment transport, but the exact impact is not well known. Therefore governmental as well as local measures involving hydraulic structures to counter beach erosion have been taken along the Yucatán coast.

One of the predominant mitigation measures taken by local property owners along the coast to prevent beach erosion is the construction of so-called espolones, or self-made groins constructed out of timber and rocks, as displayed in figure 2. Groins are one of the oldest forms of coastal protection structures, and are used in multiple ways and forms around the world. Generally, groins can be described as solid, shore-normal constructed structures, emplaced for the purpose of maintaining the beach behind them or controlling the amount of sand moving alongshore (Kraus & Hanson, 1994). However, application of impermeable groins, the most found type of groin along the coast of Yucatán, tends to stimulate rip currents and seaward loss of sand around the groin, and most of all stimulate downdrift erosion alongshore (Bakker, 1984). However, making groins permeable may be a solution to the downdrift problem caused by impermeable groins. As discussed in a paper by Otay et al. (1997), permeable groins may cause the deposition of sediment to be equal on the updrift and the downdrift side of the groin. Therefore, permeable groins might remove the negative effects of downdrift erosion seen in applications with impermeable groins.



Figure 2. Example of an impermeable groin on the beach of Progreso, Yucatán. With a longshore wave direction moving from right to left in the picture, accretion on the right (updrift) side is visible, whilst the left (downdrift) side suffers from erosion due to the sediment blocking groin (*photographed by author*).

1.3 Problem definition

While impermeable groins have been studied intensively, the application of permeable groins has received much attention from researchers. Research into groins has been focused on big coastal structures such as seawalls and piers (Lira-Pantoja et al., 2012; Medellin et al., 2015) or using groins as a method to estimate longshore sediment transport (Wang & Kraus, 1999), but not as a measure of erosion prevention.

In the spring of 2015, a field experiment has been conducted by LIPC to investigate coastal dynamics and sediment transport processes around an impermeable groin in Sisal, Yucatán. By using a 14.4-m impermeable groin (as used by Wang & Kraus, 1999) during one sea-breeze event, measurements have been taken for the longshore sediment transport. However, the effects of a permeable groin during strong sea-breeze conditions have not been tested under natural conditions in this area.

1.4 Research aim and research questions

The aim of the research is to investigate the impact of a permeable groin on beach morphodynamics in Sisal, Yucatán, and assess its capability to prevent beach erosion. During an experimental investigation, a permeable groin is deployed during strong sea-breeze events and its impact on beach morphology is compared with the impact of an impermeable groin deployed in the previous study.

The main research question which has to be answered in the research is as follows:

What is the impact of a permeable groin on beach in Sisal, Yucatán before and after its deployment during strong sea-breeze events and how can it be applied as a measure to prevent beach erosion?

In order to answer the main research question, five sub-questions have been formulated:

- 1. What is the natural variability of beach morphology during strong sea-breeze events?**
- 2. What is the volumetric change of the beach induced by the presence of a permeable groin on the up- and downdrift side during one sea-breeze event of 24h?**
- 3. What is the beach resilience after removal of the permeable groin?**
- 4. What is the impact of a permeable groin on the up- and downdrift side of the beach in comparison to an impermeable groin?**
- 5. How can the application of a permeable groin help in beach recovery and how should the design of the groin be improved for use in everyday applications?**

1.5 Reading guide

In the following chapters of this report, an answer will be given to the main research question. First of all, a description of the study area is given in chapter 2, followed by a description of sediment transport processes and their theory in chapter 3. Chapter 4 contains a description of the execution of the field experiment and an overview of how all results of the field experiment were processed. Chapter 5 discusses the obtained results in two parts: the first part gives a clear description of the natural variability in the study area, while the second part discusses the changes occurring with the implementation of a permeable groin during one sea-breeze event. The report concludes with a discussion in chapter 6 and the conclusion in chapter 7.

2. Study area

Sisal ($21^{\circ}10'06''$ LN and $90^{\circ}01'30''$ NW, figure 1) is a small fishing village located at the northern coast of the Yucatán peninsula. It is situated in the Hunucmá municipality in the state of Yucatán, and is about 50 km northwest of the state capital Mérida. It was the principal port for the state of Yucatán from 16th century until the 19th century, until the establishment of the port of Progreso made Sisal obsolete. Sisal has a wide beach, contrary to many other beaches along the Yucatán coast.

The northern coast of the Yucatán peninsula is characterized as a low-lying coastal area with 861.6 km of coast, consisting of 58.6% coastal lagoons and 41.4% coastal front, of which 84% is sandy coast front (CINVESTAV, 2007). Sediment characteristics of the beach fronts are only available for the Progreso coastal front, reporting ranges between 0.2 mm (at 0.5 m depth) and 0.5 mm in the swash zone with poorly sorted grains. (Uc-Sánchez, 2009). Reported median grain sizes for the Sisal area range from 0.28 mm on the beach front to 0.53 mm in the surf zone (Wellmann, 2014).



Figure 3. View of the beachfront at the experimental site in Sisal. Note in the picture on the right the large berm, often a characteristic of microtidal beaches (photographed by author).

The tidal regime in the Sisal beach area is a microtidal environment, i.e. a tidal regime with a mean tidal range less than 2 m. The area in which the Sisal beach is situated, is subject to a mixed tidal regime with a predominant diurnal tide regime with tide ranges varying between 0.1 m for neap tides and 0.8 m for spring tides (Cuevas-Jiménez and Euán-Ávila, 2009), such that tidal influences on beach morphodynamics may safely be ignored. Microtidal beaches are often characterized by a large berm marking the transition from the beach to the swash zone, as visible in figure 3 (Scott et al., 2011). The study area is located between two breakwater structures: the Sisal Pier on the east side of the beach and the jetty, which forms the entrance to the port of Sisal on the other side, generating an oscillating shoreline between the jetty and the pier (Torres-Freyermuth, p.c.)

The study area is characterized by its deepwater low-energy wave conditions due to the presence of a large continental shelf, also called the Yucatán Shelf. This wide and shallow shelf, visible in figure 4, is up to 245 km wide and has a nearly monotonic slope of 1/1000 to 1/2000 (Enriquez et al., 2010). The wide and shallow continental shelf causes sheltering from the swell introduced by the Caribbean Sea (Appendini et al., 2012). Therefore, locally generated short period waves propagate towards the coast and the slope of the shelf decreases wave energy, inducing wave-breaking near the shoreline (Medellin et al., 2015). Typical values for significant wave height (H_s) were reported to be around 0.4 m for the area around Sisal (Appendini et al., 2012).

Despite the deepwater low-energy wave conditions, the study area is subject to high wave events. Caused by strong diurnal sea-breeze events throughout the year, these sea-breezes often cause heavy swell of waves despite the low-energy wave conditions. The sea-breezes start in the late morning/beginning of the afternoon and decrease again around the beginning of the evening (local time). In this period, the sea-breezes are at its most intense. Wind speeds can reach an average of 20 m/s during an intense sea-breeze event, increasing wave height, especially in the later afternoon (local time) when highly energetic wind waves reach the shoreline.

For the Sisal area, during diurnal sea-breeze events, winds hit the shore from a predominantly northeast (NE) orientation, indicating a high incidence angle relative to the coastal orientation. However, strong wave-conditions are not always solely driven by strong wind conditions. As concluded by Enriquez et al. (2010), the currents over the Yucatán shelf are modulated and influenced not only by strong sea breezes, but also by the momentum gained from the Yucatán current. The Yucatan Current flows adjacent to the coast from the Yucatan Channel, located between the Yucatán Peninsula and the Cuban coast, to the direction of Progreso/Sisal influenced by the general circulation characteristics in the eastern part of the Gulf of Mexico.

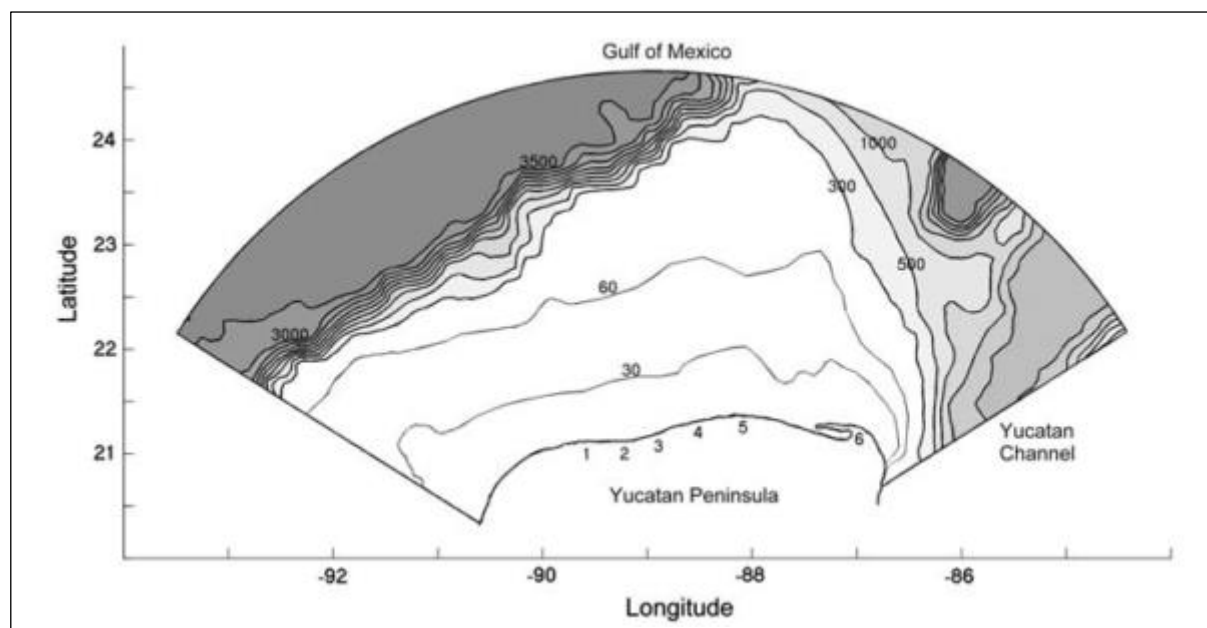


Figure 4. Map of the Yucatan Shelf (Campeche Bank) showing bottom topography. Also the locations of Progreso (1) until Cabo Catoche (6) are visible at the coast (Enriquez et al., 2010)

3. Theoretical background

In this chapter, the theoretical background will be given. This theory overview is based on descriptions given by the Shore Protection Manual (USACE, 1991, 2001), Marine Dynamics (Ribberink, n.d.) and papers mentioned in the text.

3.1 Wind waves

Due to its geographical position, the mainly unstable atmosphere of the Eastern Gulf of México play a key role in the high wind speeds and highly directional nature of wind seen on the north and north-east coasts of the Yucatán peninsula (Soler-Bientz, 2010). Strong sea breezes develop in the early afternoon causing the wind to change to an onshore north-east breeze, changing to an alongshore easterly breeze as the Coriolis force takes effect.

Deepwater waves are affected by the wind, as transfer of momentum and energy takes place between wind and deepwater waves through friction proportional to the square of the wind speed, and wind waves start to propagate relative to the direction of the wind (Open University, 1999). Energy picked up from wind by the wave depends on fetch, or the unobstructed distance from the origin of the wave to the coast. In open sea, waves not only get energy from winds (potential energy), but also velocity from currents which drive masses of water (kinetic energy). Energy obtained by wind waves per unit area E (J/m^2) is described as a function of water density ρ (kg/m^3), gravitational acceleration g (m/s^2) and wave height H (m) (USACE, 2001):

$$E = E_{kin} + E_{pot} = \frac{1}{16}\rho g H^2 + \frac{1}{16}\rho g H^2 = \frac{1}{8}\rho g H^2 \quad (3.1)$$

Wave energy is propagated through a propagation velocity c_g , caused by hydrodynamic pressure and velocity of motion of water particles. As a result the transported flux of wave energy through a plane of unit width is related to equation 3.1 in accordance with linear wave theory (Ribberink, n.d.):

$$F = E c_g \quad (3.2)$$

When deepwater wind waves enter shallow water, the waves are affected by the decreasing depth. Typically, waves are affected when their speed is less than 1/20th of their wavelength. In shallow water, energy propagation velocity is affected by the shallow depth as a product of gravitational acceleration and local depth d_b (USACE, 2001):

$$c_g = \sqrt{gd_b} \quad (3.3)$$

In order to maintain a constant energy flux in the nearshore zone, the decreasing propagation velocity has to be compensated. Visible in equation 3.4, as gravitational acceleration and water density remain constant, compensating a decreasing velocity is done by an increase in wave height. This process is called shoaling, and explains the increase in wave height in the nearshore area.

$$\frac{\partial F}{\partial x} = 0 \rightarrow \frac{\partial}{\partial x}(E c_g) = 0 \rightarrow \frac{1}{8}\rho g H^2 c_g = \text{constant} \quad (3.4)$$

Not only energy propagation velocity and wave height is affected by the shallow water, but also wave direction θ is affected. Wave angle starts to change in accordance with Snell's law as $\frac{\sin(\theta)}{c_g} = \text{constant}$ (Longuet-Higgins, 1970). This process is called refraction, and shows that when wave speed starts to decrease due to the effects of shoaling, wave angle in the nearshore area also starts to change. Longuet-Higgins (1970) showed that wave flux in the cross-shore direction is

affected by the changing wave angle in accordance to equation 3.5, assuming a monotone beach slope increase:

$$F = Ec_g \cos(\theta) \quad (3.5)$$

Commonly, when wave height reaches 0.78 times the local water depth, waves start breaking (Wiggels, 1978). Breaking occurs, because the top of the wave starts overtaking the bottom of the wave and starts to spill forward. Variations in wave height in cross-shore direction due to the effects of shoaling and refraction in the nearshore area, lead to variations in wave energy flux. The total cross-shore wave energy flux may therefore be written as a combination of equation 3.1, 3.2, 3.3, 3.6 and the breaker parameter $\gamma_b = H_b/d_b$, with H_b as the breaking wave height (USACE, 1991):

$$F_{CS} = \frac{1}{8} \rho g H_b^2 \left(g \frac{H_b}{\gamma_b} \right)^{0.5} \cos(\theta) \quad (3.6)$$

After breaking, the wave height starts to decrease and the decrease in wave flux is balanced by a return current or undertow, flowing offshore and on the bottom in the surf zone.

3.2 Sediment transport due to wave action

Motion of sediment particles influenced by wave action is induced by cross-shore and alongshore motion. Cross-shore transport occurs with normal wave action, stirring up sediment and transporting sediment either onshore or offshore. However, when oblique waves break, wave force is not only induced in the cross-shore direction, but also in the longshore direction, causing a net longshore current which transports sediment with it. The movement of sediment along the zone close to the shoreline or littoral zone is referred to as longshore sediment transport or littoral transport, with the actual volumes of sediment referred to as littoral drift.

A distinction is made between two modes of sediment transport: suspended sediment transport and bed-load transport. When sediment is transported and is carried above the bottom by turbulent eddies in the water, the mode is classified as suspended sediment transport. When sediment transports itself while staying close to the bed and move by rolling and saltating, the mode is classified as bed-load transport.

3.2.1 Cross-shore sediment transport

As waves enter shallow water, they begin to lose speed due to shoaling and friction, increasing wave height. As the wave crest spills forward, large accelerations caused by toppling and breaking of the waves generate strong horizontal pressure gradients that act on the sediment, generating friction (Hoefel, 2003). The friction at the bottom stirs up sediment due to velocity differences between water layers, generating turbulence which forces sediment to move (Ribberink, n.d.). Mostly, cross-shore sediment transport occurs when hydrodynamic changes occur in the nearshore zone, resulting in an imbalance due to modified forces in the bed, thus causing movement of sediment and profile change.

Constructive forces are the forces that tend to cause onshore sediment transport, thus increasing the sediment budget in the nearshore zone and causing accretion of the beaches. These forces occur in normal wave action under calm circumstances when waves with relatively low energy approach the coast, creating bottom shear stress pointed towards the coast (USACE, 2001).

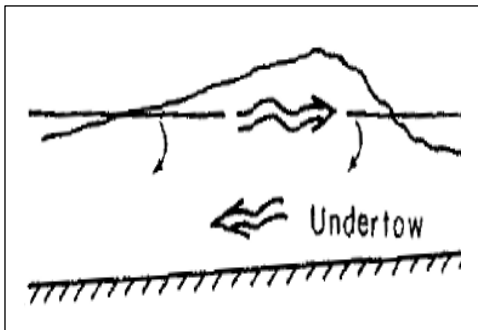


Figure 5. An example of undertow (UCSB, 2016)

Destructive forces are forces that tend to cause offshore pointed sediment transport and develop during high-energy wave action (Hoefel, 2003). These forces are mostly related to the vertical structure of the cross-shore currents, most importantly regarding velocity profiles and mass balance, or may concern normal physical behavior, such as gravity. One of the most common destructive forces is undertow, or the seaward return flow of wave mass transport, visible in figure 5. When waves break and topple, they push mass and energy downward, slowing the flow of water in the lower regions of the velocity profile, up to a point where the seaward pointed pressure causes a seaward velocity along the bed. The seaward velocity induces a seaward pointed stress on the sediment in the particles, moving sediment in the seaward direction (USACE, 2001).

3.2.2 Longshore sediment transport

As mentioned before, waves in most cases do not break shore-normal, but break obliquely. The

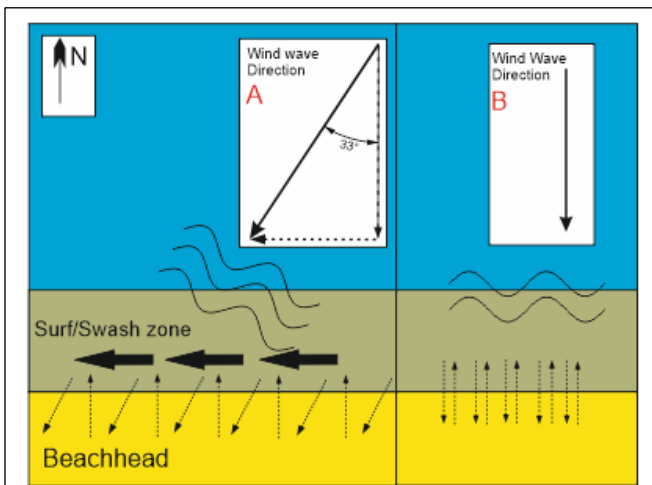


Figure 6. Visualization of longshore sediment transport (solid black arrows) at a 33 degree angle of attack (a) and 0 angle of attack (b).

obliquely breaking waves are often a result of refraction and shoaling. These waves release a momentum in the cross- and alongshore direction at the shore when they break. A release of momentum in the alongshore direction of the velocity gives rise to a longshore current, driving sediment longshore, as can be seen in figure 6. Therefore, the angle in which waves break at the coast (θ_b) is an important parameter in the determination of strength and direction of littoral transport. The magnitude of littoral transport Q_{LT} is dependent on a diverse pallet of parameters, but may be described in principle as a product of concentration

$c(z)$ and velocity $u(z)$ in time in a plane of unit depth h , with water elevation η , and width as described by Güner et al. (2011), assuming an average wave propagation over time:

$$Q_{LT} = \int_0^{h+\eta} c(z) u(z) dz \quad (3.7)$$

Velocity is dependent of wave forces, wave angle and radiation stresses. Sediment concentration on the other hand is dependent on size of sediment material in the littoral zone. In coastal areas, wave action severely stirs up material from the bottom which in turn is transported by velocity (Van der Velden, 1989). Sediment is most often stirred up by turbulent vortices and is suspended in the water as an immersed weight. Therefore, sediment transport rates may be calculated as an immersed weight transport rate I_l related to the volume transport rate by the mass density of the sediment grains ρ_s (kg/m³), water density, gravitational acceleration and the in-place sediment porosity n :

$$Q_{LT} = \frac{I_l}{(\rho_s - \rho)g(1 - n)} \quad (3.8)$$

The immersed weight transport rate is related to the wave energy flux by a factor described by Galvin (1979). The relationship by Galvin relates the longshore transport rate to the energy flux of waves. The relationship is based on the concept of energy-based longshore transport through wave energy, and is a function of an empirically defined dimensionless sediment coefficient K and the alongshore component of wave energy flux F_{al} :

$$I_l = K F_{al} \quad (3.9)$$

Combining the equations 3.8 and 3.9, assuming that the angle in which the waves refract is the same angle as the one the waves break ($\theta = \theta_b$), and denoting that the alongshore component of the wave energy flux F_{al} is formulated by $F_{al} = F_{CS} \sin(\theta)$:

$$\begin{aligned} Q_{LT} &= \frac{K}{(\rho_s - \rho)g(1 - n)} F = \frac{K}{(\rho_s - \rho)g(1 - n)} \frac{1}{8} \rho g H_b^2 \left(g \frac{H_b}{\gamma_b} \right)^{0.5} \cos(\theta_b) \sin(\theta_b) \\ &= \frac{K}{16(\rho_s - \rho)(1 - n) \sqrt{\gamma_b}} \rho \sqrt{g} H_b^{5/2} \sin(2\theta_b) \end{aligned} \quad (3.10)$$

Equation 3.10 displays one of the most used formulas in longshore transport: the CERC-formula, developed by the Coastal Engineering Research Center in 1966 (USACE, 1966, Hanson & Kraus, 1991). It gives a good idea and an adequate description of the total littoral transport rate when assuming suspended sediment transport. However, in recent years it was found that the CERC-formula over-predicts sediment transport rate and alternatives were developed. One frequently used alternative is the experimentally tested and theoretically established Kamphuis-formula (Kamphuis, 1991) which predicts the longshore transport based on parameters such as the median grain size of the beach D_{50} , the wave period T_p , significant wave height at breaking H_{sb} and the beach slope m_b :

$$Q_{LT} = 2.27 H_{sb}^2 T_p^{3/2} m_b^{3/4} D_{50}^{-1/4} \sin^{3/5}(2\theta_b) \quad (3.10)$$

3.3 Shoreline change due to divergence of longshore sediment flux

The longshore and cross-shore processes described above are heavily intertwined with each other in the nearshore zone. A variation in one may cause a big variation in the other, and vice versa. Longshore current might be one of the biggest displacers of sediment in the nearshore zone, but the combination of both longshore and cross-shore transport ultimately is decisive in the accretion or erosion of a beach, heavily influenced by diverse parameters such as wind speed, wind direction, wave height, and wave direction.

When a groin or breakwater is introduced into the coastal system however, there might be quite some changes in the nearshore area, especially regarding longshore sediment flux. Groins introduced in the nearshore area are often placed for the purpose of maintaining the beach (1) or controlling the amount of sand moving alongshore (2) (Hanson & Kraus, 1990). These impermeable structures force accretion on updrift side of the structure by trapping sediment displaced by the longshore current, most often by blocking the flow of sediment in the longshore direction. By blocking the longshore sediment flow, the direct downdrift side of the structure is deprived of sediment budget. The cross-shore transport interacts with the changed profile, often accreting the

updrift side whilst eroding the downdrift side due to the lessened sediment budget on the downdrift side, caused by the blockage of littoral drift. The major accretion on the updrift side (figure 7, D) therefore is ‘balanced’ by a massive erosion directly downdrift of the structure (figure 7, E), causing the characteristic ‘sawtooth’ shape of the beach.

As longshore transport is diverted around the structure, high difference in velocity gradients at the seaward side of the structure occur due to hindrance of the longshore current. These high velocity gradients between the calmer flowing and partially blocked updrift side and the free flowing downdrift side often causes heavy turbulence and the occurrence of rip currents near the downdrift side, leading to more erosion on the downdrift side (Bakker, 1984).

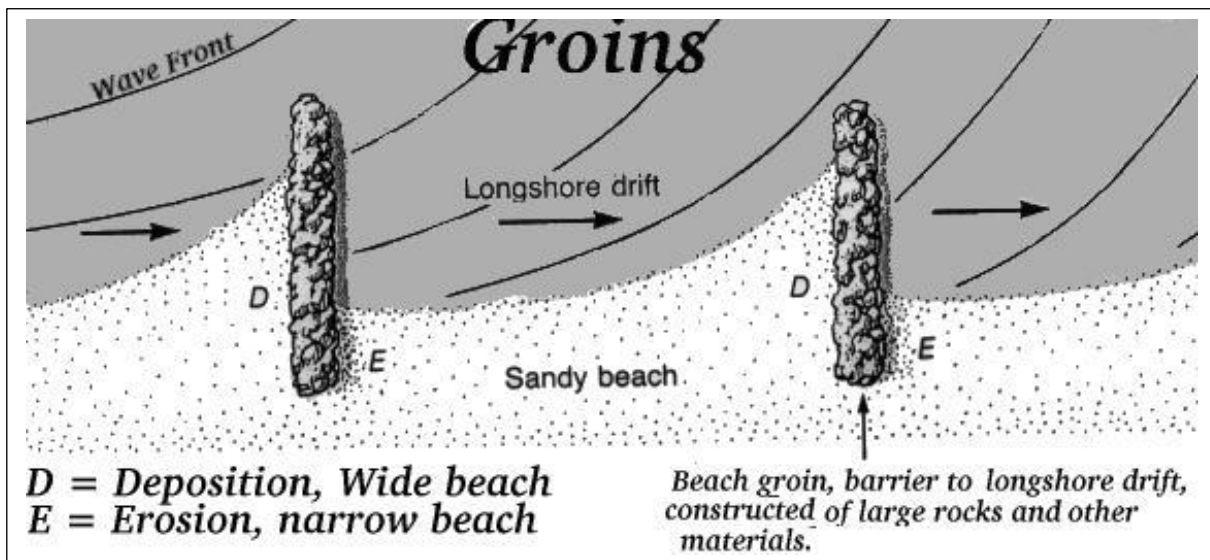


Figure 7. Development of shoreline around an impermeable groin (UCSB, 2016).

Semi-permeable or even fully permeable groins therefore may offer a solution to the downdrift erosion problem. Permeable structures allow for partly passing of longshore currents, in turn transporting sediment from the updrift to the downdrift side of a structure and balancing sediment budgets on both parts of the structure. Therefore, the introduction of a (semi)-permeable structure in coastal systems offer a more continuous beach line and a more gradual velocity gradient and less turbulence near the downdrift side of the groin (Bakker, 1984).

4. Methodology

In this chapter, an overview will be given of the methodology for the field experiment and subsequent data analysis. For more detailed information about the instruments used in the experiment, please refer to Appendix A.

4.1 Experiment setup and structure design

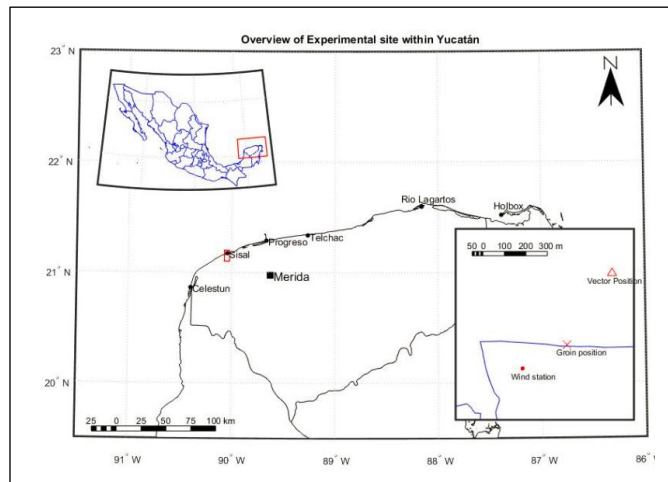


Figure 8. Overview of experimental site in the Yucatán area.

The experiment took place along the Sisal beach front along the north coast of the Yucatán Peninsula. The field experiment consisted of deploying a permeable structure on the Sisal beach. A quick overview of the experiment location is given in figure 8.

Data regarding changes in beach profile were obtained by measuring beach profiles using RTK survey along 21 surveying lines or transects, 10 transects on the updrift side of the groin, marked 1-10, and 10 transects on the downdrift side of the structure, marked 12-21. The middle transect (11) marked the location of the permeable groin (see figure 9). Transects were set up in a telescopic grid with increasing distances, symmetrical in the up- and downdrift direction. Transects closest to the groin are 2 m apart, extending to 15 m for the outermost transects.

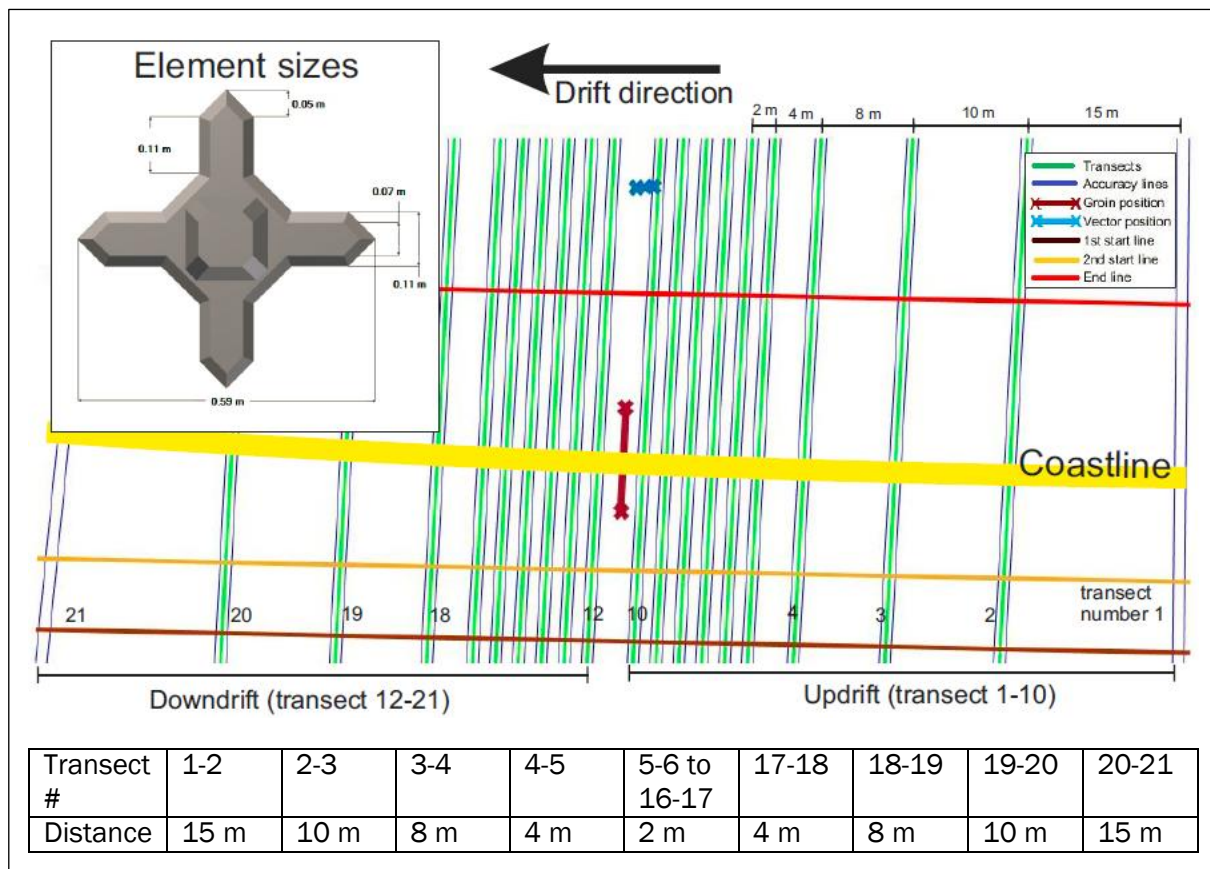


Figure 9. Overview of field experiment site with position of instruments and the groin, and an overview of terminology used regarding the experimental site. Also, dimensions of the elements used are given in the upper left corner and distance between transects is given.

All measurements were conducted in the same procedure. Firstly, the height at a control point was measured. This control point was always a fixed point at a non-changing location. Next, bed profile along each transect was measured, starting with the outermost updrift transect (1) and finishing with the outermost downdrift transect (21). Around all transects were ‘accuracy limits’ of 50 cm to the left and to the right defined in which during RTK surveys the surveyor was required to stay for a good positional accuracy. Afterwards the control point was measured again, ensuring that any changes in the setup were corrected for. More about the corrections can be read in section 4.1.3.

On the morning of the 31st of May 2016, the groin was built up out of 72 elements. Construction of the groin was started at 6:30 local time and was finished around 8:00 in the morning. The elements are around 0.59 m long and high, a width of 0.53 m (as visible in the inset in figure 9) and weighing around 60 kg each, ensuring stability against wave action. These elements were stacked in three rows: the first row extending the full length from the beachhead to the surf zone, comprising of 42 elements with a total length of 15 m, interlocked as in figure 10a. The second row started in the swash zone and extended to the surf zone, comprising of 18 elements, interlocked with each other as in figure 10a, and interlocked with the first row as in figure 10c. The third row was a layer on top of the first and second row, extending the height of the structure up to 0.9 m, consisted of 12 elements, and was interlocked with the first and second row visible in figure 10b. The elements were interlocked using a cross-pattern, which allowed for sediment bypass. The height of the structure allowed water overtopping, but the length of the structure ensured water could only pass by overtopping or passing through the structure.

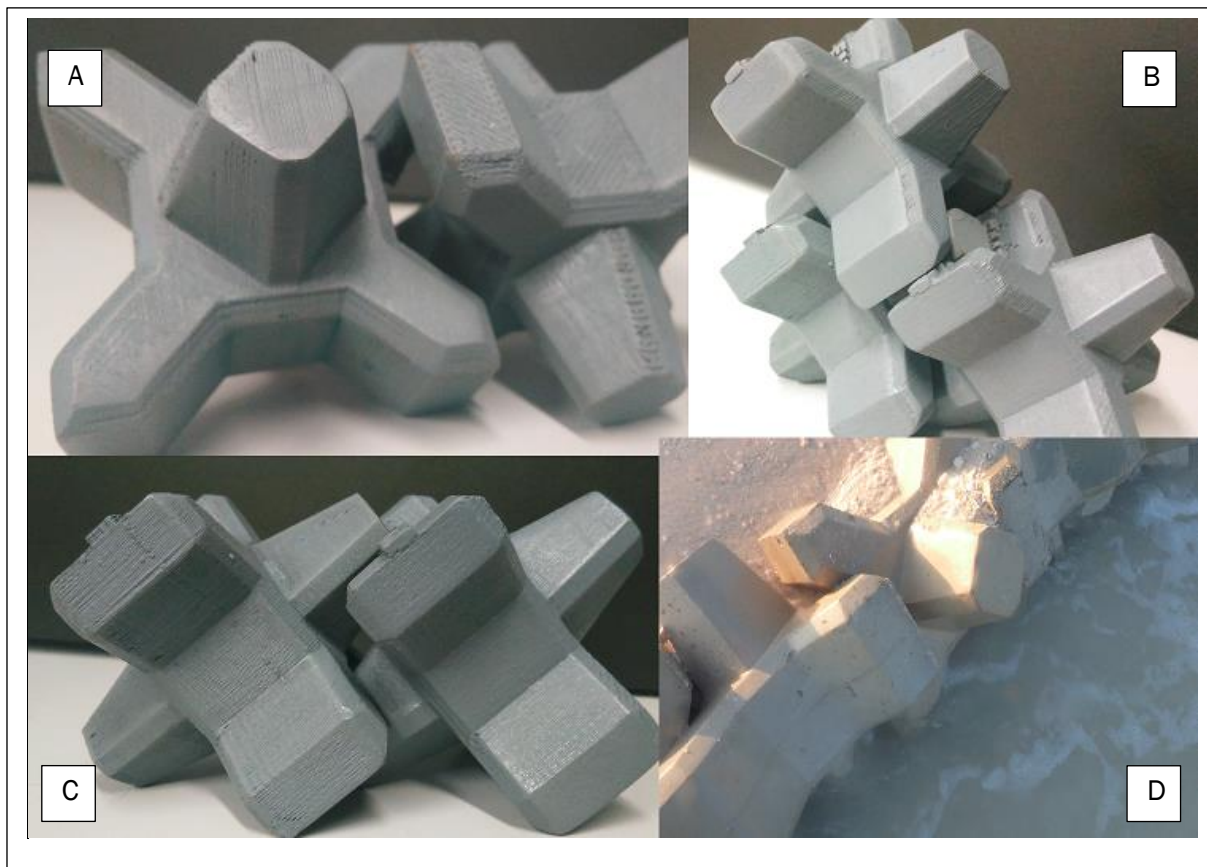


Figure 10. Images of the groin setup with interlocking of the elements. Counterclockwise: (A) shows the interlocking between elements next to each other, (C) shows the interlocking of the first row with the second row, (D) shows the element interlocking during the field experiment with the sediment passing holes filled up, and (B) shows the second layer setup on top of the first layer (*photographed by author*).

4.2 Measurements of conditions

More detailed information regarding the measurement equipment can be found in Appendix A.

4.2.1 Beach profile and beach conditions

Beach profile measurements were conducted by RTK (Real Time Kinematic) survey using the LEICA GS14/CS15 GPS/GNSS system, a position data survey technique using global navigation satellite systems (GNSS) to determine position and height using phase differences in signals coming in from satellites relative to a receiver. The measurements were conducted for different purposes termed as: inter-day measurements, experimental measurements, post-measurements and intra-day measurements, which can be found below. All times noted are local time.

Measurement #	Start	End	Remarks
PRE 01	17:10	18:30	Conducted at 11-05. First measurement with the Leica
PRE 02	10:10	11:30	Conducted at 18-05
PRE 03	10:30	11:45	Conducted at 23-05
PRE 04	10:20	11:30	Conducted at 27-05

Table 1. Overview of taken inter-day measurements.

The inter-day measurements were conducted in the weeks before the experiments and were meant to monitor long-term variability. Most of inter-day measurements were also used to become familiar with the equipment used during the experiment.

Measurement #	Start	End	Remarks
01	08:15	09:23	ADV distance (08:20) 48 cm from bed
02	10:00	10:56	ADV distance (10:30) 50 cm from bed
03	12:10	13:07	ADV distance (12:17) 50 cm from bed
04	14:20	15:20	ADV distance (14:30) 52 cm from bed
05	16:05	17:05	ADV distance (16:20) 53,5 cm from bed
06	18:00	18:50	ADV distance (18:20) 56 cm from bed
07	20:15	21:15	-
08	22:00	01:19	Lots of problems with RTK survey datalink to the base, constantly losing signal. Problem (partially) solved at 1:00
09	01:50	02:45	-
10	03:55	04:59	Accidentally switched transect 16 and 17 in measurement
11	05:57	06:52	Forgot transect 17. Was added as transect 20 at 06:45
12	08:10	09:20	ADV distance (08:40) 52 cm from bed

Table 2. Overview of measurements during the experiment run-time.

Twelve measurements were conducted during the 24h-experiment. After construction of the groin was finished, work began on the pre-survey (#1), determining the baseline for the measurements. During the 24h-run, the surveys were conducted every other hour. Around 8:30 on the 1st of June, the structure was removed and the post-survey (#12) was conducted. During measurements, some problems occurred regarding the equipment, therefore no survey could be held at 00:00.

Measurement #	Start	End	Remarks
POST 1	12:30	13:40	First post-deploy measurement, 4 hours after removal
POST 2	10:10	11:10	Second post-deploy measurement, 24 hours after removal
CHANGE 1	11:15	12:20	First change measurement, morning of 15-06
CHANGE 2	17:10	17:50	Second measurement at afternoon of 15-06
CHANGE 3	10:05	11:15	Third measurement, morning of 16-06
CHANGE 4	17:00	18:05	Final measurement, afternoon of 16-06

Table 3. Overview of post-measurements for beach resilience and change measurements.

Post-deployment measurements were conducted 4 and 24 hours after removal of the structure. Unfortunately, no other surveys could be done due to problems with the equipment. The post-deployment measurements were conducted to assess beach resilience. Measurements concerning the intra-day variability were conducted a week after removal of the structure. During two days, four measurements were taken in the morning and the afternoon to assess the natural variability occurring during daytime on transects.

4.2.2 Wave, wind and current data

Wave climate measurements were conducted with a Nortek Vector ADV. The Nortek Vector is an Acoustic Doppler Velocimeter (ADV) that uses the principle of the Doppler Effect in order to assess water speed. During the experiment, one Vector was deployed in the outer surf zone about 50 m offshore in a depth of 2 m. Due to the limited storage capacity of this Vector ADV, it could only be deployed for two days, starting at 6:30 on the 31st, and ending at around 12:00 at the 2nd of June. Wave and current measurements were taken around 50 cm from the bed, ensuring a fully submersible Vector at all times throughout the 24-hour period.

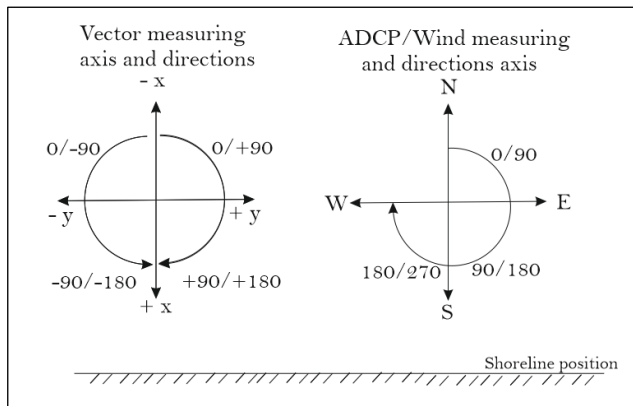


Figure 11. Axes setup for the instruments used.

Long-term wave data was obtained from an Advanced Doppler Current Profiler (ADCP), located 1.5 km offshore at a depth of 4 m. Wave data from the ADCP is used to obtain information regarding the long-term variability in significant wave height and current speed and direction, providing a framework for data obtained from the Vector ADV. Wind data was obtained from a wind station located on top of the institute building, giving an indication about short- and long-term variability of wind speed and wind direction.

As figure 11 shows the measurement axes for the different instruments, the direction measured by the instruments are to be differently interpreted. Current direction obtained from the Vector ADV and current direction obtained from the ADCP and shows a directional heading or the direction in which the current flows. Wind direction obtained by the wind station show an originating heading, or the direction of which the current originates. When referring to data on an X-Y-Z plane, the x-axis is defined as the cross-shore component, the y-axis as the alongshore component, and the z-axis as the height component.

4.3 Data reduction and correction

4.3.1. Data reduction for wave data

Wave data reduction and calculation consisted of (1) determination of significant wave height and (2) determination of current direction.

Significant wave height was determined using two methods, as used by Sharpe (1990). The first method is taking an average over 1 minute using the highest third of the N number of measured waves. Significant wave height is here defined in the time domain. The second method is taking the waves that are four times the standard deviation (σ_n) or variance (m_0) of the surface elevation, or equivalently as four times the square root of the zeroth-order area of the wave spectrum. The significant wave height as defined in the frequency domain is H_{m0} , and described:

$$H_{m0} = 4\sqrt{m_0} = 4\sigma_n \quad (4.2)$$

Whilst the ADCP current data could be directly obtained, current data from the Vector had to be analyzed for current direction. This was done through conversion of the Cartesian coordinates found in the velocity components to Polar coordinates, revealing wave direction through analysis of the velocity components.

4.3.2. Data reduction for survey data

Survey data reduction and calculation of changes in beach profile consisted of (1) correcting data for errors found in survey data, (2) calculating profile-volume in the measurement period and (3) calculating total volume accumulation on the up- and downdrift side.

(1) Correction of survey data was necessary, because of occurrence of errors in height data. While positional accuracy in the X-Y plane using RTK surveying is measured accurately with an error margin of 3 mm, height depends strongly on equipment set-up at that time. When walking with a mobile rover, tilting of the rover occurs due to unexpected movement. The tilt causes the rover to register a height slightly less than the actual height. Also, because the rover was carried on the back of the observer in a backpack, errors in height occurred due to tilt by walking and fit of the backpack. Therefore, height is corrected through the following procedure: a predefined point for the measurement $H_{GPS,m}$ is accurately measured and registered. Each survey, the control point is measured beforehand ($H_{GPS,c1}$) and afterwards ($H_{GPS,c2}$) using the equipment setup at that moment. The height measured at a data point H_i was then corrected according to:

$$H_{new} = H_i - \left(\frac{H_{GPS,i1} + H_{GPS,i2}}{2} - H_{GPS,m} \right) \quad (4.3)$$

Not only might there be inaccuracies in height, but also in position relative to transects and to the starting point. It causes inaccuracies in the distance compared to the relative starting point, because during the measurements, it is not possible to ensure position to be exactly on the transect, hence the accuracy lines around each transect. To correct the distance of the datapoint relative to the transect, the following formula was used, where x_i and y_i are the alongshore (X) and cross-shore (Y) coordinates of datapoint i , and x_1 and y_1 are the alongshore (X) and cross-shore (Y) coordinate of the starting points:

$$d = \sqrt{(x_i - x_1)^2 + (y_i - y_1)^2} \quad (4.4)$$

(2) Calculating total volume gain per transect v is done by using numerical integration using the trapezoidal method as seen in equation (4.5) along a set interval, ranging from a cross-shore distance of 5 m (y_1) to 30 m (y_2). This interval was chosen, because this interval reflects all points between a depth of +0.5 and -1, updrift and downdrift. This interval was also chosen because of its reflection of the area of the transect in which the most change can be witnessed, and these volumes are changes relative to the first defined measurement. The trapezoidal rule is applied with a non-uniform grid, calculating transect volume v as a product of the space between two points in the cross-shore direction ($y_{i+1} - y_i$) and the height ($z(y_{i+1}) + z(y_i)$) associated with those points:

$$\int_{y_1}^{y_2} v(y) dy \approx \frac{1}{2} \sum_{i=1}^N (y_{i+1} - y_i) (z(y_{i+1}) + z(y_i)) \quad (4.5)$$

(3) Volume gains were calculated as the volumetric gain along transect v_i over its influence area defined by the starting points on the second starting line ($x_{s,i+1} - x_{s,i}$). The influence area is defined as the space between two transect as shown in figure 9. The volume was first corrected to see change relative to the first defined measurement, and was next multiplied by its influence area, as visible in equation (4.6):

$$V_{LST} = \sum_{i=1}^N (x_{s,i+1} - x_{s,i}) v_i \quad (4.6)$$

4.3.3 Establishing bandwidth to assess natural variability

In order to assess natural variability, a bandwidth was empirically established by investigating the value of intra-day variability, and assessing for all transects what the percentage of exceeding the threshold values of the bandwidth was, the threshold values being certain upper and lower limits for bed level change over time.

The empirical bandwidth was established as a check to investigate whether transects are affected by the presence of a structure or not. If a transect does not exceed the empirical 10% threshold value, it is assumed that 90% or more of the measured points bed level change fall within the established bandwidth, and only natural variability plays an influence on that specific transect. However, if a transect exceeds the empirical threshold of 10%, and thus less than 90% of the measured points fall within the established bandwidth, it is assumed that the specific transect is influenced by the presence of a structure. The 90% value was used as a safeguard to compensate for occurring anomalies in the data.

The bandwidth was empirically established using the intra-day difference in bed level. The intra-day difference in bed level was used as it best reflected the intra-day measurements that were taken during the experiment period. Firstly, natural bed level variability was obtained by correcting all measured points per transect with respect to the mean of the intra-day difference in bed level of that transect. Next, the bed level variability was checked against empirically established upper and lower limit values. The percentage per transect of the number of values exceeding that upper limit and the percentage per transect of the number of values exceeding that lower limit was calculated as $(N_{values\ exceeding\ threshold} - N_{total\ values}) * 100\%$. If at least 90% of the values fell within the upper limit AND if at least 90% of the values fell within the lower limit, the bandwidth was accepted as the bandwidth for natural bed level variability.

One important note: in chapters 5.1.3 and 5.2.2, numerous references to ‘variability’ and ‘change’ are made. When referring to ‘variability’, a reference is made to a difference between a measured value at a certain point in time and the average over time of values on that point. When referring to ‘change’, a reference is made to a difference between a measured value at a certain point in time relative to its first measured value on that point. Thus, variability is a time average difference, and change is a difference between the first and current measured value at that point.

5. Results

In this chapter, the results will be discussed. Keep in mind that the data is plotted for GMT and not corrected for local time. The local time is GMT -6 and when discussed in the text, it is made clear what the local and GMT times are.

5.1 Natural variability

5.1.1. Wind

In figure 12, a representation of sea-breeze events over ten days is given. As may be witnessed in this figure, the sea breeze event starts when winds start picking up around 10:00 (16:00 GMT) in the morning. The winds rapidly increase in intensity and start blowing at a constant rate. The highest average speeds are reached during the late afternoon (around 23:00 GMT), after which the winds rapidly decrease in speed. Wind direction normally do not vary much and are within the spectrum 'North-South'. During the sea-breeze events, the winds mostly arrive from the east, indicating a longshore wind direction relative to the beachfront in Sisal. During non-sea-breeze events, winds originate from the landward direction.

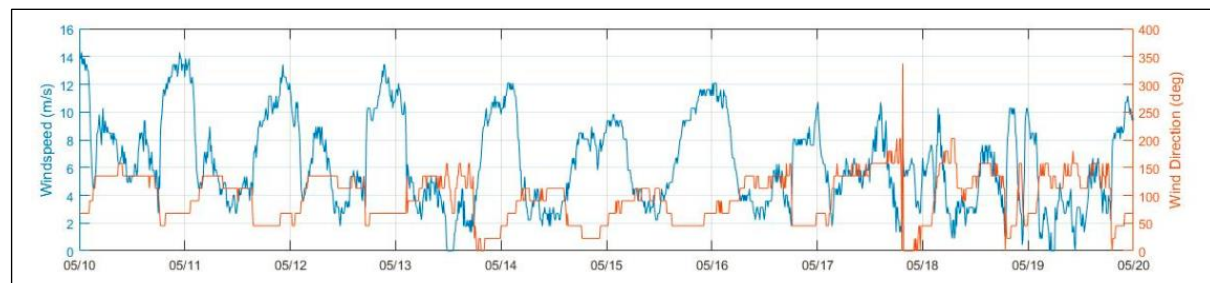


Figure 12. Wind speed and wind direction measured during 10 days, from 10 to 20 May.

During these sea-breeze events however, as mentioned before, winds are quite intense and energetic. Therefore, they might affect wave energy, especially if the waves are under constant influence from wind during their movement their origin to the coast. Therefore, sea-breezes might explain the occurrence of larger waves during sea-breeze events, as waves along the fetch pick up more energy through wind. During these sea-breeze events however, as mentioned before, winds are quite intense and energetic. Therefore, they might affect wave energy, especially if the waves are under constant influence from wind during their movement their origin to the coast.

5.1.2 Waves

One of the most dominant factors concerning the displacement of sediment in the longshore direction is the action generated by waves. As shown in chapter 3, wave height and wave angle are important parameters in determining the rate of littoral transport. Wave height directly affects the wave energy and thus the displacement of sediment in the bed, while wave angle determines the rate and direction of longshore transport. Data about wave angle and height was obtained from an ADCP marooned at a depth of 4 m, 1.5 km offshore from the experiment site.

Although the connection between wind and wave height might not be clear from theory, when looking at figure 13a, a clear correlation can be seen between wind speed and wave height over time. During the day, wave height follows a similar pattern as wind speed. When wind speeds start picking up at around 18:00 (12:00 local), a direct increase in wave height can be witnessed. At the peak of the sea breezes, wave height is at its maximum and decreases as wind speed decreases.

A correlation of 0.79 was found in figure 13a for 10 days of data, indicating a strongly correlated connection between wind speed and significant wave height.

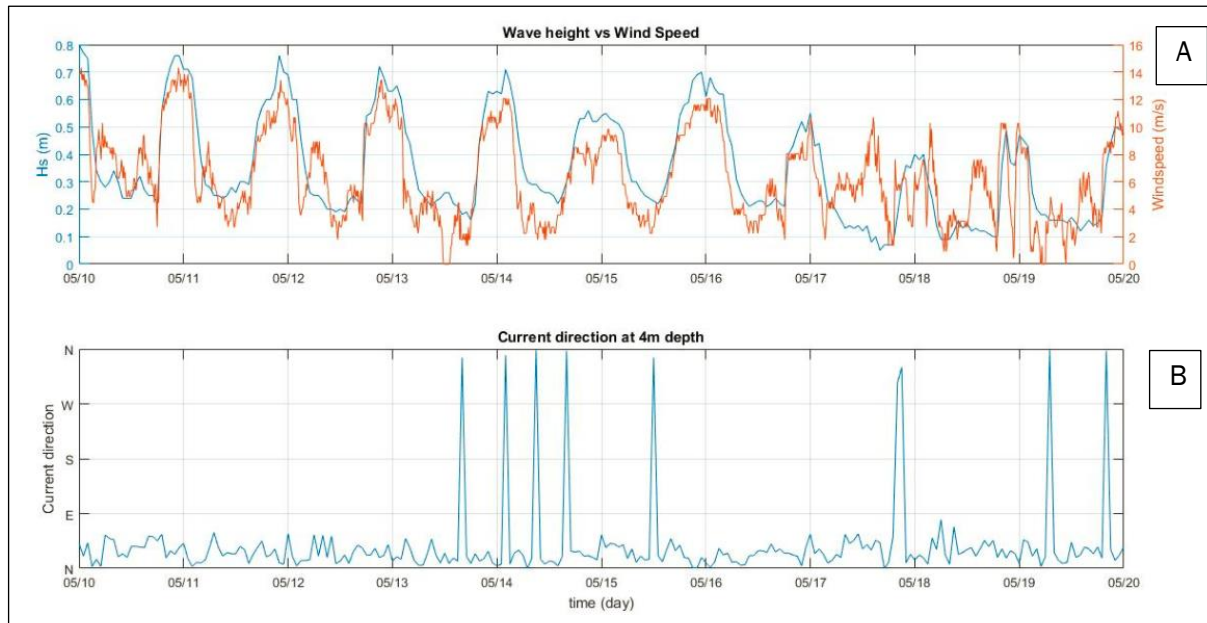


Figure 13. (a) Significant wave height plotted versus wind speed and (b) current direction during 10 days.

Current angle, or the angle in which the wave current approaches the coast, is visible in figure 13b. The angle of the current at 1.5 km offshore is on average 35 degrees, indicating a northeast pointed current. This direction contradicts with the expected longshore direction heading west. As pointed out by Enriquez et al. (2010), currents in the offshore region on the northern coast of the Yucatán Peninsula are not only influenced by tides and winds, but also by the momentum gained from the Yucatán Current, explained in chapter 2. The current obtained through the ADCP shows that deep-water currents are affected by the Yucatán Current, whereas shallow water directional measurements like the ADV show currents induced by wave breaking.

5.1.3 Beach morphology

With the influence of wind and waves, the beachfront is constantly shifting. During nighttime, accretion of the beaches through mild wave conditions occur, whilst during the day the beaches erode due to strong waves carried by the sea-breeze events. These occurrences do not only bring changes in the beach profile intra-day, but also in the long run these changes might affect the shape of the beach.

As Sisal is a microtidal beach, one characteristic is a large berm in front of the swash zone. Figure 14b displays the course of a typical bed level profile, in which different characteristics are visible. The berm starts around 0.7 m above sea level and causes a sudden drop to 0.1 m, and declining until the start of the swash zone at 0 m and mean sea level at -0.3m. From the swash zone, the steep beach slope continues into the surf zone until reaching a depth of about -1.3 m. Here, the shelf begins with a slope far less compared to the surf zone slope. Large morphological changes due to wave action therefore mostly imply the zone starting from the bottom of the berm and extending all the way until the depth of closure. Around 30 to 40 m offshore, small sand banks can be detected in the bed level, their position varying on a day-to-day basis.

During the day, strong sea-breeze events have a strong eroding effect on the beach. The intra-day variability¹ is immediately noticeable when looking at the example of transect 10 in figure 14, showing variance of bed level over the course of two days. During the course of the day, accretion and erosion patterns in transects differ per transect location and with intensity of the diurnal sea-breeze event.

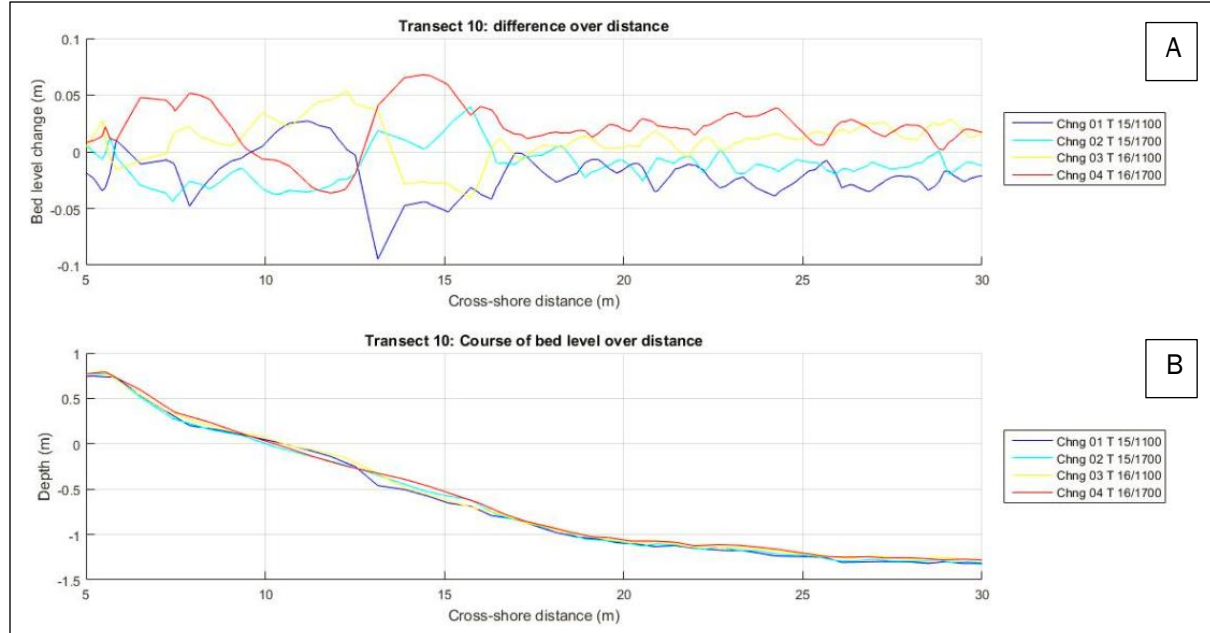


Figure 14. (a) Intra-day variability of bed level in transect 10 and (b) the course of bed level profile of transect 10 over two days.

The difference erosion and accretion is also witnessed in the inter-day variability, the variability of transects over a longer period of time. Looking closely at figure 15, a similar pattern of accretion and erosion can be witnessed in the nearshore area. Under sea-breeze conditions, the shoreline often oscillates between the Sisal jetty and the Sisal pier (Torres-Freyermuth, p.c.). As the measured site is located in between the Sisal jetty and pier, such variability remains small compared to the areas close to the pier and the jetty. It implies that at the measured site due to oscillation in the shoreline position, no net erosion or accretion occurs and that natural variability of the beach for the most part will depend on the intensity of the diurnal sea-breezes.

An equilibrium in shoreline over the course of multiple days is also suggested by the alongshore evolution of the shoreline visible in figure 15². Whilst during the period of pre-measurements the shoreline in longshore direction slightly erodes, later on during the inter-day change measurements the shoreline recovers to its old position. The position of the shoreline, especially at an isobath of minus 0.3 m height, is heavily influenced by the intensity of sea-breeze events, showing change up to a different degree alongshore. Difference in alongshore and cross-shore change might be explained by the difference in local sediment transport gradients due to alteration of waves and their energy fluxes by shoaling and refraction in accordance to equations (3.3) and (3.5).

¹ Due to disturbances in measurements, only the updrift transects (1-10) for the intra-day variability could be measured with a good accuracy. Therefore, when discussing the intra-day variability, only the updrift transects are used to determine the intra-day variability.

² See footnote 1

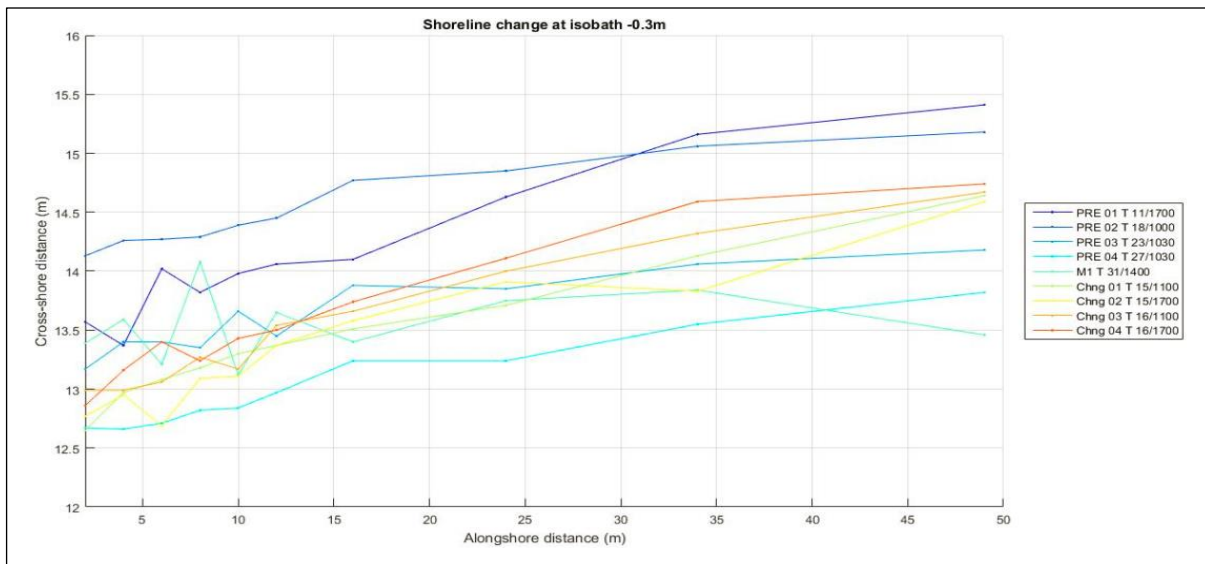


Figure 15. Shoreline position at an isobath of -0.3 m for the inter- and intra-day measurements on the updrift side of the groin. The groin is located at an alongshore distance of 0 m.

For the study area, a suggested equilibrium might indicate that if a structure is introduced into the system, changes in bed level would fall out of the daily accretion and erosion range of natural variability and suggest the presence of a sediment trapping structure. Looking back at figure 14a, one may notice that the values for bed level change over time in all transects fall within a certain range. A bandwidth was empirically established for the bed level variability per transect as a range of values in which at least 90% of all measured differences in bed level fall, in accordance with the method in chapter 4.3.2.

This bandwidth was found to be valid for bed level variability ranging from a positive bed level threshold of 0.09 m to a negative bed level threshold of -0.09 m. As the established bandwidth was found for the intra-day variability data, the empirical bandwidth was validated by data taken from the inter-day variability, as visible in figure 16. It suggests that bed level change over a short period of time as well as a long period of time mostly falls within the same bandwidth.

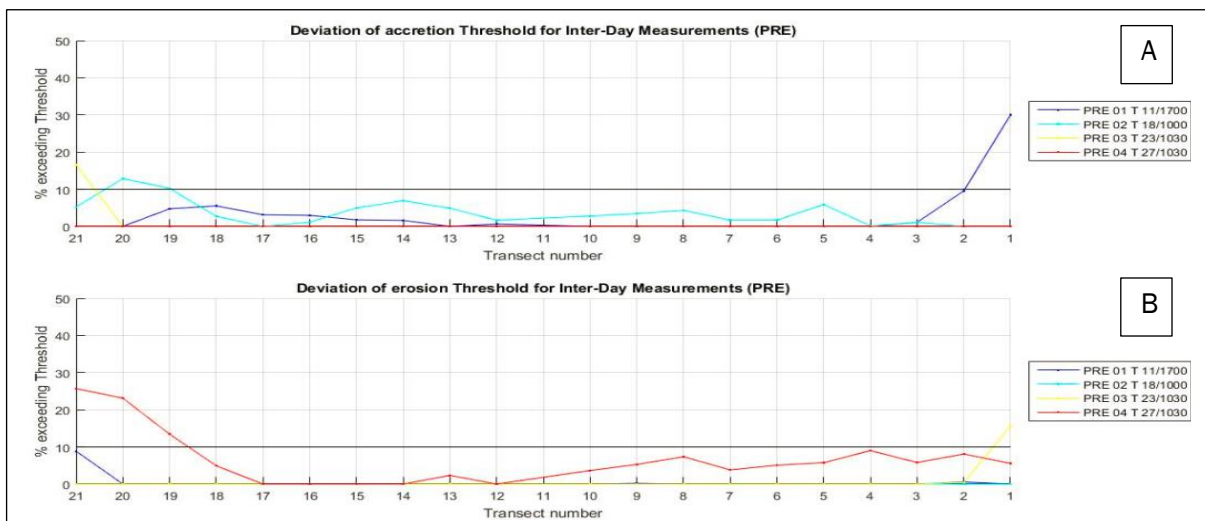


Figure 16. Percentage of deviation of (a) accretion threshold of + 0.09 m bed level difference and (b) erosion threshold of - 0.09 m bed level difference for the intra-day measurements.

5.2 Impact of a permeable groin during one sea-breeze event

5.2.1 Forcing conditions during the experiment period

Wind conditions

During the 24h-run of the groin, as explained in section 4.1, the wind conditions were typical for a sea-breeze event. The average wind speed was around 6.71 m/s. The dominant wind direction was east-south-east during the calm periods, while the strongest winds originate from the north-east, east-north-east and east directions. Figures 17a and b indicate that during the sea-breeze period, the winds mostly came from north-east, hence indicating a positive effect of wind direction on wave development in the longshore direction. The calmer winds mostly occurred during night time.

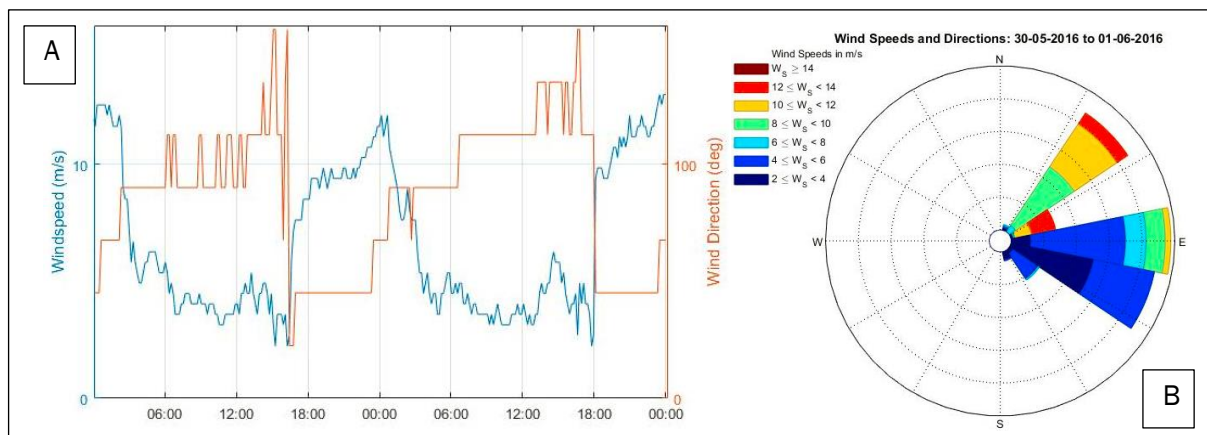


Figure 17. (a) Wind speed and wind direction and (b) predominant wind directions during the experiment period.

Wave and current conditions

Wave conditions have been measured over 48 hours using the Nortek Vector ADV. Deployment began at 7:00 local time (13:00 GMT) in the morning at the 31st, and ended around 12:00 (18:00 GMT) at the 2nd of July. During this period, the Vector was able to register two sea breeze events, one on the day of the field experiment, and one on the day after. When looking at figure 18, in which the significant wave height is plotted, the significant wave height showed a big increase under sea-breeze conditions, and significant wave height can be seen increasing from an average of 0.16 m to almost 0.35 m in under two hours. While wind speeds pick up around 17:30 (11:30 local), wave height is seen to increase almost half an hour later, and starts picking up around 18:00 (12:00 local). Significant wave height during the experiment shows a regular pattern during a sea-breeze event. Mean significant wave height for the two sea-breeze periods is 0.21 m, with maximum wave height around 0.39 m above mean sea level.

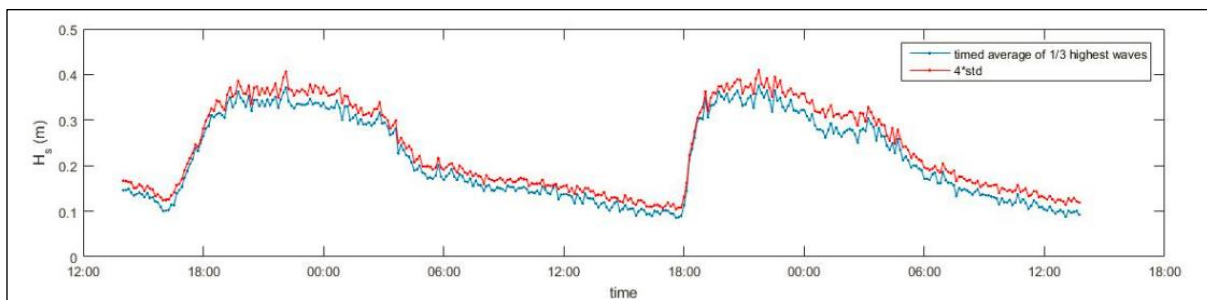


Figure 18. Significant wave height during the experiment period obtained with the 1/3rd highest wave method (blue) and the 4 times standard deviation method (red).

In figure 19, the velocities in the cross-shore (x) and the alongshore (y) direction is displayed along with the significant wave height. Both velocity components seem affected by the sea breeze, further establishing the connection between the sea breezes and wave energy. The positive and negative signs are always indicated relative to the axis directions as in figure 11.

The cross-shore velocity shows speed above and below zero, reaching from a maximum of 0.05 m/s to a minimum of -0.13 m/s, with a mean of -0.03 m/s. During calm conditions, the cross-shore velocity mostly seems on-land indicated by the positive values. However, during sea-breeze conditions, a negative velocity develops and becomes more intense with the increase of the wave height, indicating the presence of undertow. This may be explained due to the distribution of flow velocities over wave height. In order to preserve a mass balance over the complete wave, a positive forward velocity component due to spilling and breaking of waves is compensated by a rearward pointed velocity component near the bed, thus ensuring the mass balance to be in check (USACE, 2001).

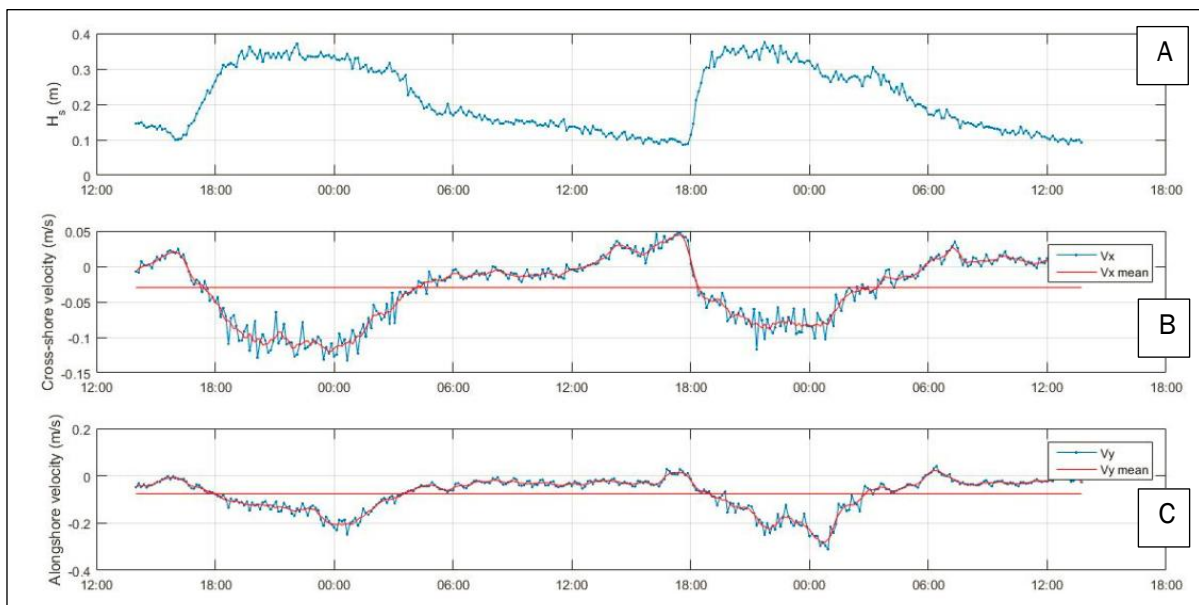


Figure 19. Significant wave height (a) versus cross-shore (b) and alongshore (c) velocity over time.

During calm events, the undertow mostly is compensated by a positive landward current. When comparing mean current speed of 0.089 m/s with the cross-shore velocity, it is indeed clear that during calm events the undertow is compensated by a landward current, however this is mostly during nighttime when winds are significantly less strong. During strong sea breezes, the undertow velocity, related to the wave height as discussed in chapter 3, induces a strong undercurrent which in turn induces a stress in the bed boundary layer, moving sediment along with it.

The longshore velocity also shows a negative value during sea-breeze events, indicating a longshore current from east to west, and a velocity of near zero during calm periods, coinciding with the low cross-shore velocities in the calm period. The large alongshore velocities during the sea breezes are explained by the current directions and current speeds found in figures 20b and 20c, which, for sea-breeze events, is pointed in the longshore direction and significantly increase during these events.

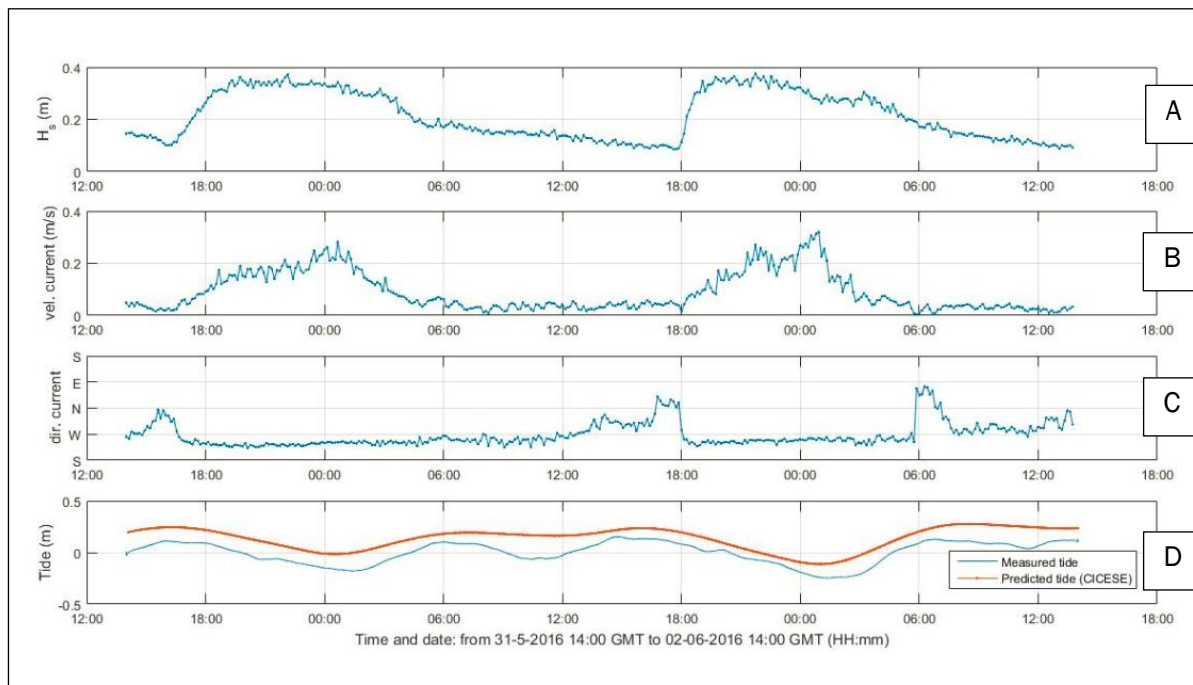


Figure 20. Plots of (a) significant wave height, (b) current velocity, (c) current direction and (d) predicted tide at Progreso (CICESE) versus measured water levels by the ADV.

Currents and tides

The current direction shown in figure 20b measured by the vector shows consistency of wave angle throughout the sea-breeze events. During these events (from 18:00 to 01:00), the wave angle is consistently seen to be around -120 to -140 degrees, corresponding to a current pointing in the southwest, alongshore direction. Tidal levels during the experiment dates ranged from -0.16 m at minimum to 0.27 m, giving a total tidal range of 0.43m during the two measurement days, which fits within the characteristic of a microtidal beach. Mean current velocity was around 0.09 m/s, with a minimum current speed of 0.003 m/s during night time and 0.32 m/s during sea-breeze events.

Currents obtained from the ADV show little resemblance to the current direction obtained from the ADCP in figure 13b. This is because the ADV, contrary to the ADCP, is stationed at the outer surf zone and therefore measures currents induced by shallow water waves. As the ADV is stationed in the outer surf zone, the current velocity in figure 20b in combination with the low local tidal gauge in figure 20d and the direction in figure 20c shows a strong onshore current during sea-breeze conditions, indicating strong stirring of the bottom layers and transportation of sediment in the onshore direction of wave propagation. During calm periods, the direction shifts to a northward pointing current in combination with a high tide. It indicates, in combination with low velocities (figure 20b), a small undertow pointed in the offshore direction.

5.2.2 Effect of groin structure on beach development

Under influence of wind, waves, tides and currents sediment is transported along the beach of Sisal. As stated before, the predominant wind- and wave direction for the nearshore area is east to south east, indicating a strong longshore transport rate in a westward direction. When encountering the experimental site, longshore current is influenced by the structure blocking its path. However, as the blocking structure is semi-permeable, it allows the current to pass through the holes between the separate elements, thus allowing a fraction of the sediment to pass as well. However, as time passes, these holes may become filled up with sediment, affecting beach profiles on the up- and downdrift of the groin.

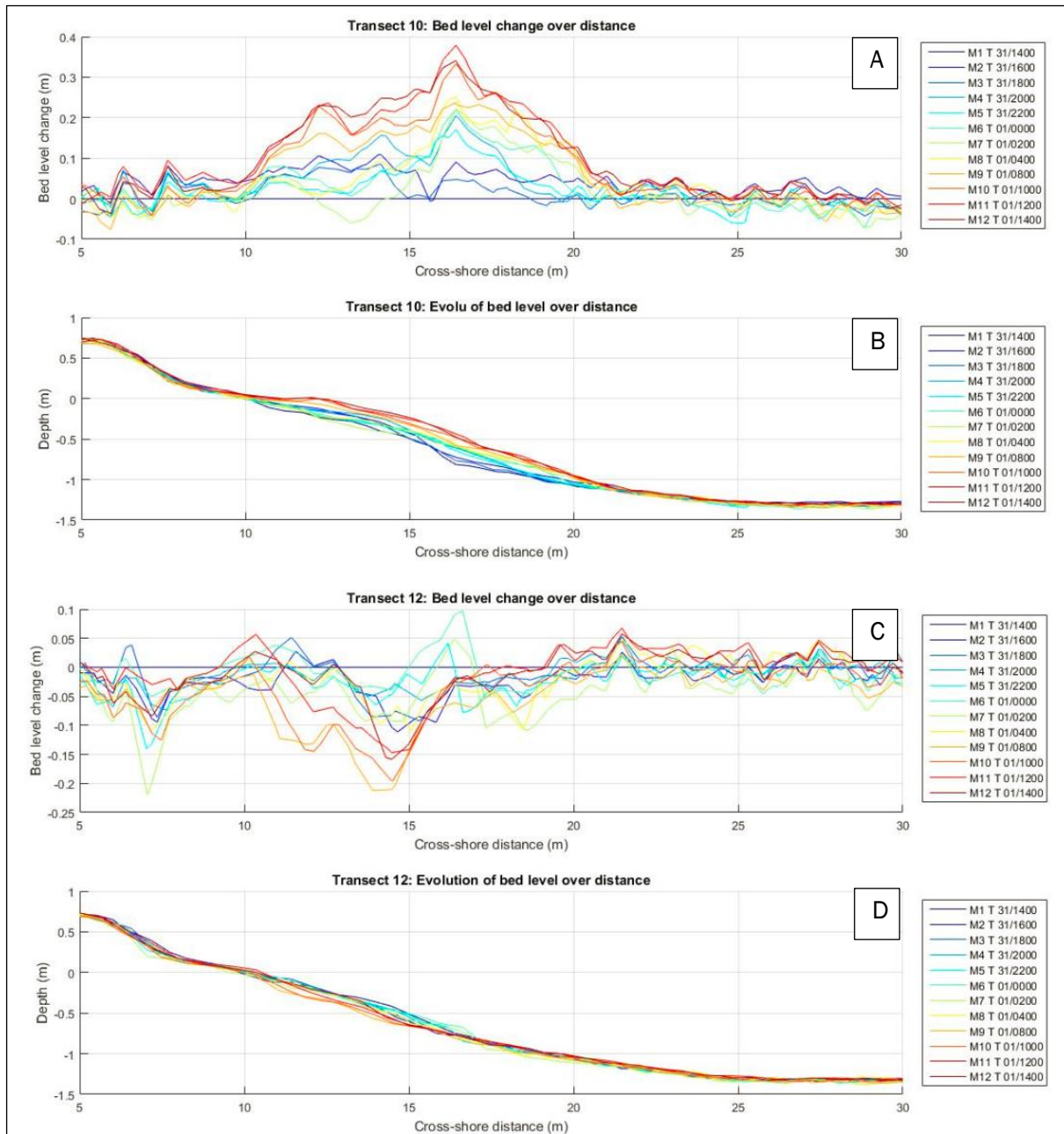


Figure 21. Bed level change over cross-shore distance in time (a,c) and evolution of bed level (b,d) for the transects 10 (directly updrift) and 12 (directly downdrift of the groin).

Although natural variability may alter the average beach profile, morphological changes around the structure are the most visible during strong sea-breeze events and are amplified when looking to the direct up- and downdrift side of the groin. When looking at transects at the direct up-

downdrift side, transect 10 and 12, in figure 21, one may notice that along the waterline, the 0 depth line, accretion on the updrift side (transect 10) is noticeable. On the downdrift side, erosion is noticeable, corresponding with the profile of an impermeable groin.

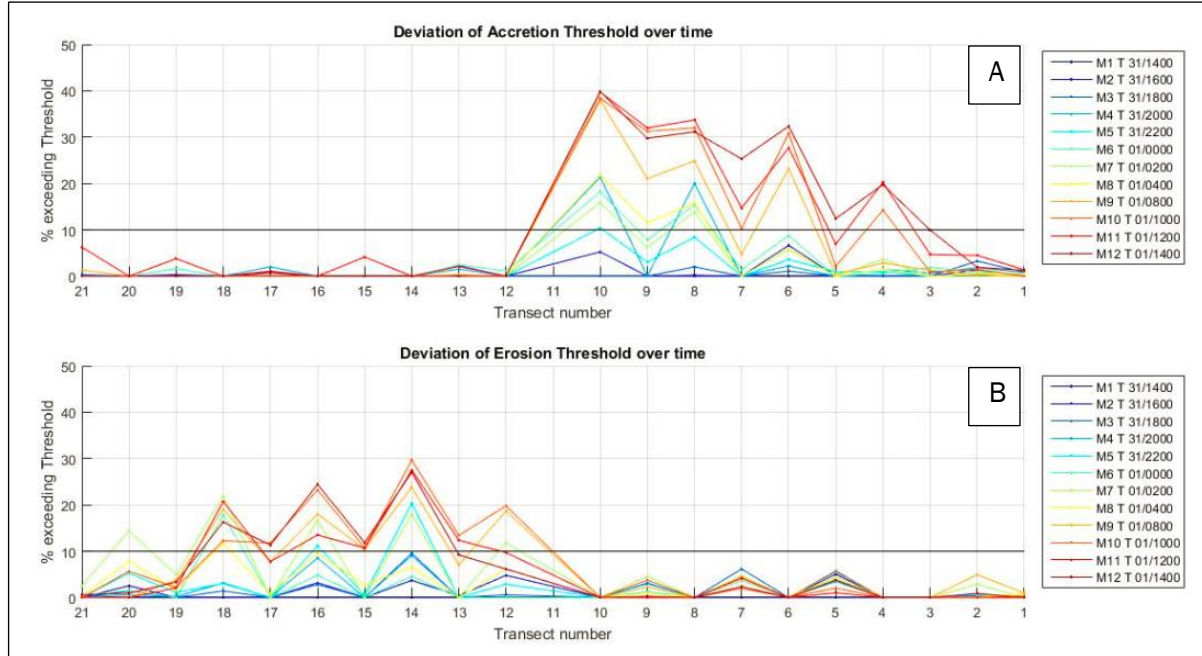


Figure 22. Percentage of deviation of the (a) accretion threshold of + 0.09 m bed level difference and (b) erosion threshold of - 0.09 m bed level difference for the measurements during the experiment period.

However, not all transects are affected by the presence of the groin, as seen in figure 22. Transects at the far up- and downdrift sides, transects 1, 2, 20 and 21, do not seem to be affected by the presence of the groin as they never exceed the established threshold. Therefore, it may be assumed that in the far up- and downdrift areas, the profile changes are assumed to be due to natural variability and thus are not affected by the presence of the groin.

Transects affected by the presence of the groin show development over the course of 24h, although the rate of accretion and erosion varies over time owing to changing wave conditions. Updrift transects (3 to 10) are increasing in volume, and the downdrift transects (12 to 19) show erosion over time. The direct downdrift transect (11) displays not only erosion, but also accretion over time, indicating a connection between the updrift and downdrift side through permeability. This seems to be confirmed by the shoreline position in figure 23b, as over time, a strongly varying rate of erosion over time is seen, implying that some of the direct downdrift erosion during calm periods is compensated by transport of sediment through the permeable groin from the updrift side to the downdrift side.

Interestingly, is the pattern of accretion and erosion does seem to change over time for multiple transects. Looking at relative change of the shoreline in figures 23 and 24, and the profile changes of the profiles in figures 21 and 22, some accretion on the downdrift side and some erosion on the downdrift side can be witnessed. Looking at current velocity, current direction and wave data, displayed in figures 19 and 20, this pattern might be explained due to the feedback between morphological changes near the structure, altering and transforming waves near the structure due to alterations in bottom profile.

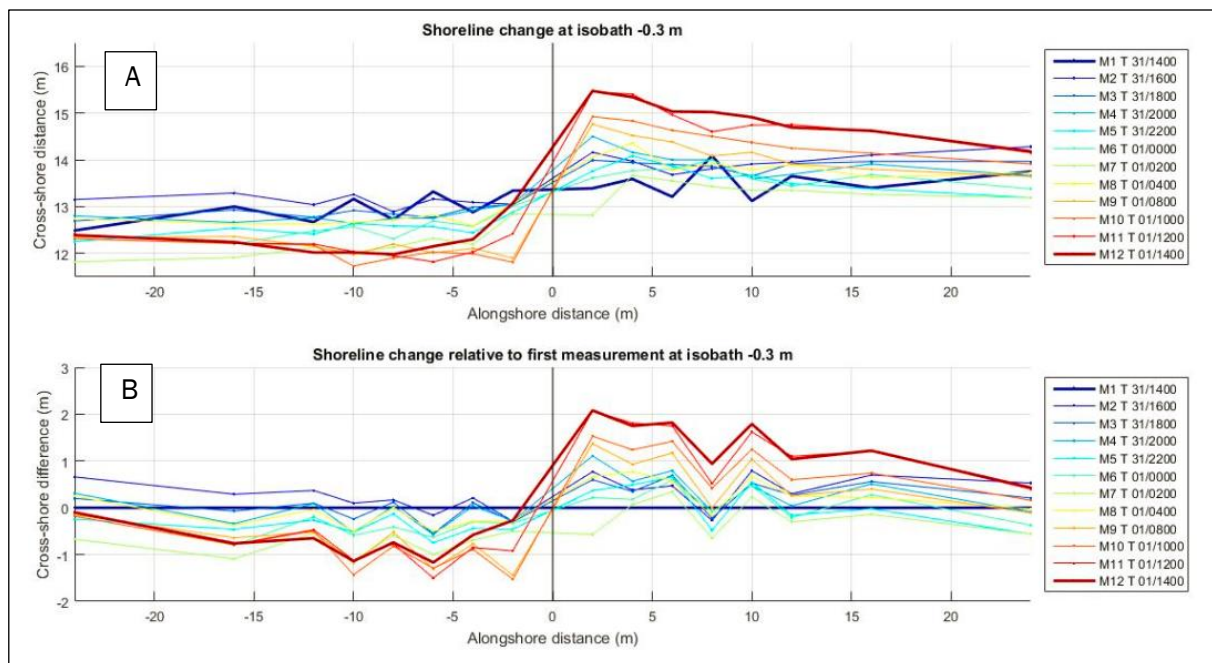


Figure 23. (a) Shoreline change and (b) shoreline change relative to the first measurement at an isobath of -0.3 m

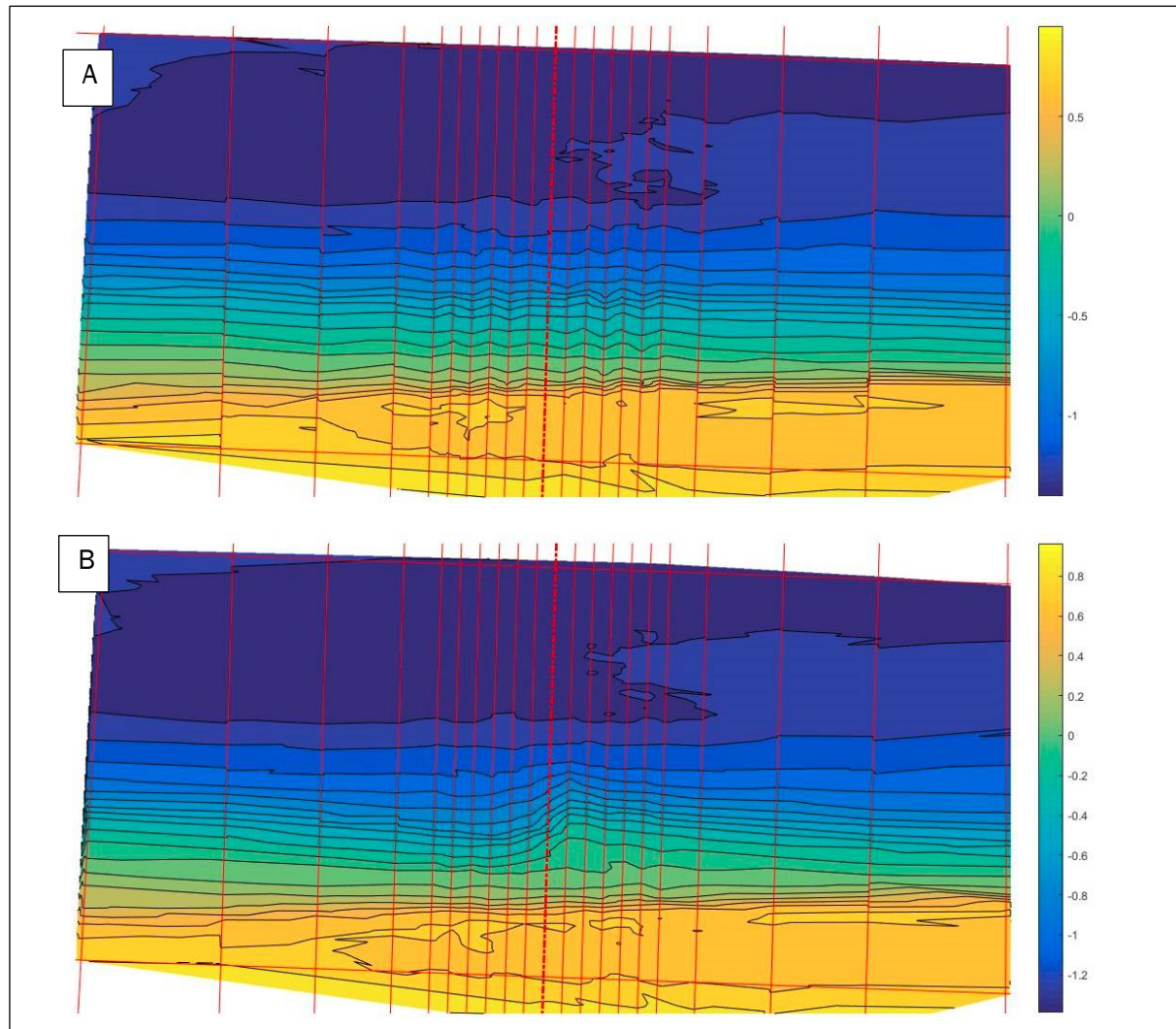


Figure 24. Contourplot of shoreline positon at (a) the start of measurements and (b) after 24 hours of structural influence. Transects are given by the red lines, with the groin positioned on the middle dotted line.

5.2.3. Volumetric change over 24 hours

Calculation of total volume gain after 24 hours is done as described in chapter 4.3.2. To assess the total volume gain, the volumetric gain after 24 hours was used and compared to the premeasurement-established volumes.

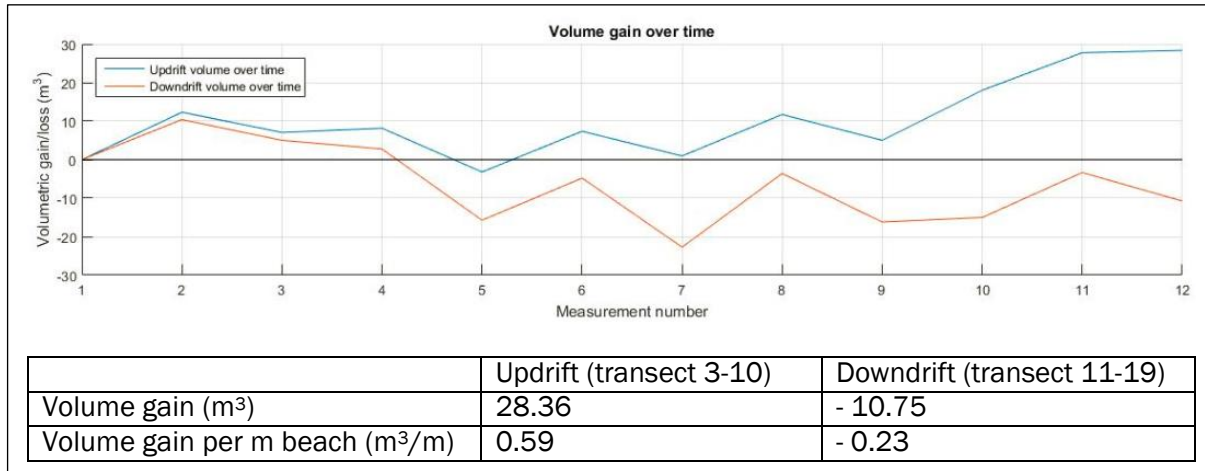


Figure 25. Volumetric gain over time (time is displayed by the measurement numbers on the x-axis).

Total captured volume over the complete area (up- and downdrift) is around 18 m³, suggesting blockage of sediment by the structure. Investigating volume gain up- and downdrift over time, figure 25 confirms the variance in the up- and downdrift pattern of erosion and accretion. During the first hours, not only the updrift side, but also the downdrift side is accreting. Longshore sediment transport is allowed to pass the groin, thus not only causing accretion on the updrift side, but also on the downdrift side. A further confirmation can be found in the fact that the variation of accretion and erosion over time seems to vary in the same direction. If the updrift side erodes over the period of two hours, the downdrift side also erodes and vice versa. It confirms a connection between the longshore transport direction and volume gain at the downdrift side. However, in the long run, when the permeability starts to decrease due to blockage of the holes by sediment, this pattern seems to fade away and starts to show a pattern similar to an impermeable groin.

5.3 Beach resilience after 24 hours

Beach resilience was measured directly after removing the groin. Beach resilience is most evident when looking at shoreline change, most notably shoreline change around the mean sea level at an isobath of -0.3 m. Figure 26 displays shoreline at four different points during the course of measurements from the first measurement (M1) until the last post-measurement (Post 02).

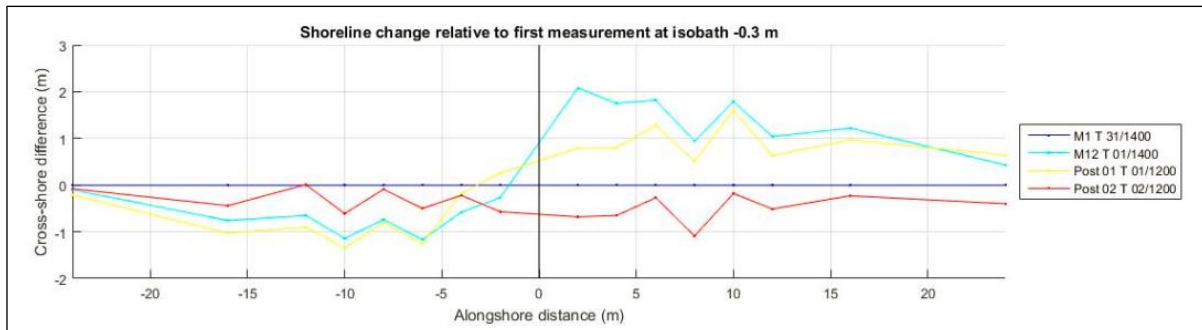


Figure 26. Shoreline change relative to the first measurement (M1) for the postmeasurements.

Looking at beach resilience, immediately noted is the big change in beach profile after 24 hours compared to the last measurement of the experiment, just before removing the structure. After 4 hours, the beach shows signs of recovery on the updrift side, however there is some more erosion on the downdrift side. After 24 hours, the beach has recovered almost completely. A shift from erosion to accretion on the downdrift side is visible as accumulated sediment from the updrift side gets transported to the downdrift side. Figure 26 shows the beach has a fast rate of restoration. Under the influence of sea-breeze events, the beach can recover from structural influence over 24 hours.

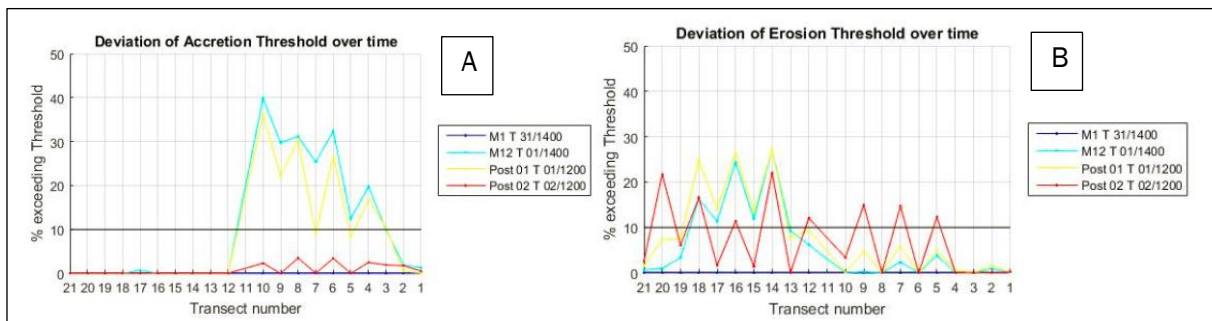


Figure 27. Percentage of deviation of the (a) accretion threshold of + 0.09 m bed level difference and (b) erosion threshold of - 0.09 m bed level difference for measurements concerning beach resilience.

The recovery of the beach after 24 hours seems to be confirmed by the deviation from the threshold for all transects compared to the first measurements seen in figure 27. No accretion is visible whilst on the downdrift side (12-19), the beach starts accreting as the deviated measurements from the negative threshold of -0.09 m starts decreasing. However, all transects do show an increased erosion, which may be caused by changed longshore transport gradients due to alterations in bottom profile.

Comparing the last post-measurement to earlier conducted measurements such as the last premeasurements, the retreat of the shoreline to a stable state is visible at the isobath line of -0.3 m, indicating that beach does not only recover from the influence of a structure within 24h, but also its recovery to a stable equilibrium state, further indicating the presence of an equilibrium beach profile and the stability of the coastline in the study area.

5.4 Shoreline change: impermeable versus permeable groin (1)

Because of the groin being permeable, thus allowing a part of the sediment to pass, shoreline change was expected to be less when compared with an impermeable groin. Also, the typical characteristics of an impermeable structure on longshore transport was expected to be less in the situation of the impermeable groin.

In figure 28, the shoreline development of the test with a permeable groin over 24 hours and the impermeable groin is shown. Data from the test with the impermeable groin confirms the test was conducted at the same location under comparable circumstances. It confirms the lesser impact the permeable groin has on the shoreline compared to an impermeable groin, with 60 m³ caught by the impermeable groin (Medellín, p.c.) and 18 m³ by the permeable groin. The rate of development of captured sediment is far less compared to the impermeable groin, and compared with the impermeable groin the permeable groin shows some sign of sediment build-up, which is to be expected due to its permeability.

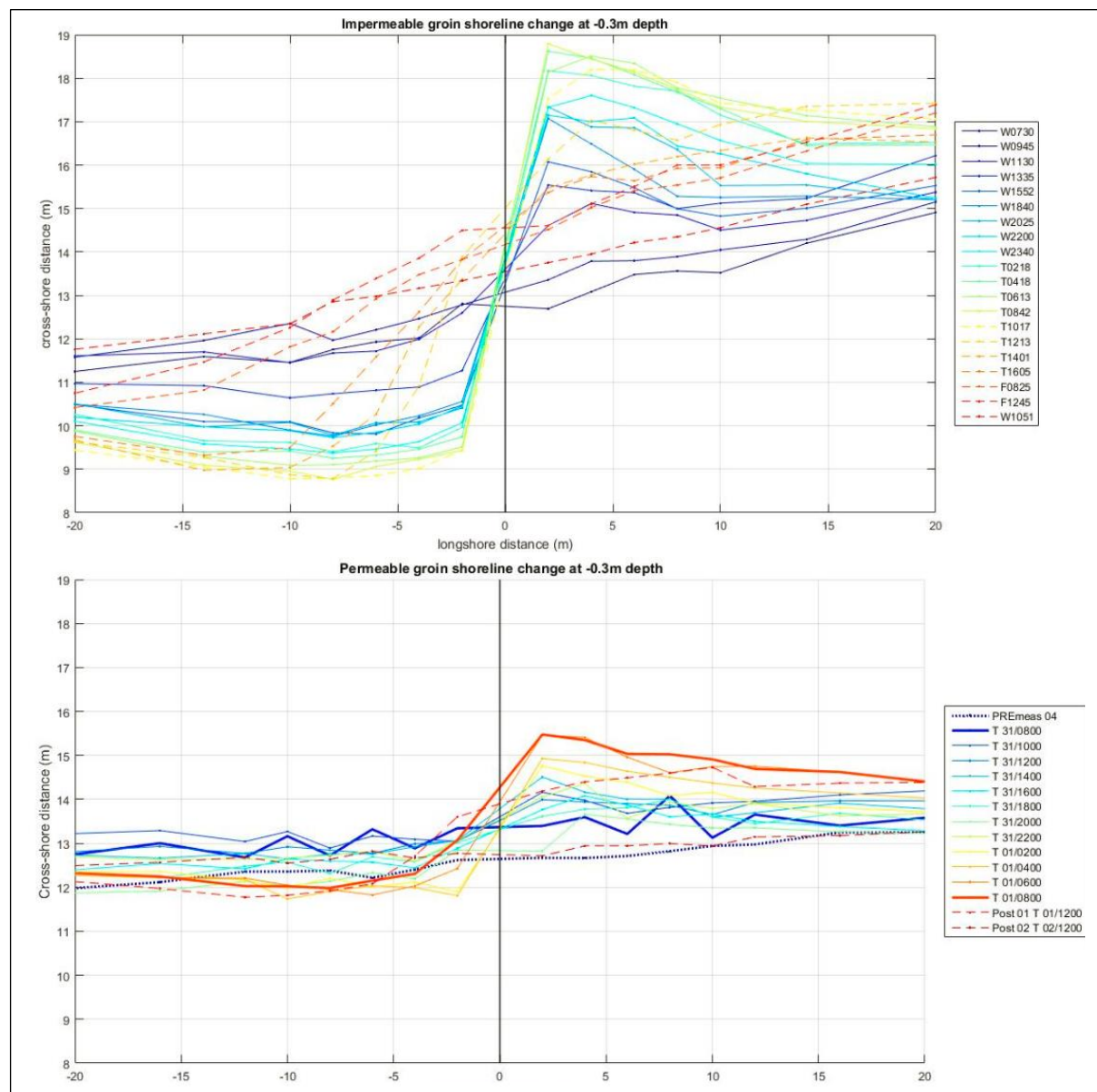


Figure 28. Shoreline change at an isobath of -0.3 m for an (a) impermeable and (b) permeable groin.

Nonetheless, the characteristic shape of the beach has not changed. Erosion for the most part happens on the downdrift side, whilst accretion dominates the updrift side. The permeable groin is more susceptible to change however, revealing a more variable pattern on both sides of the groin due to lesser sediment budget compared to an impermeable groin, revealing more sensitivity to accretion and erosion patterns. The bigger change is explained by the overtopping and passing of water and sediment through the groin.

5.5 Longshore transport rate

5.5.1 Sediment characterization

Sediment samples were taken during the course of the experiment in three different beach zones: the regular beach face, the surf zone and the swash zone. In each of these zones, two samples were taken to investigate the sediment characteristics in the area. Afterwards, the samples were dried for 48h and analyzed using high-speed camera techniques. Analysis revealed the following characteristics, as displayed in table 4.

Beach area (#)	Weight sample (g)	D ₁₀ (mm)	D ₅₀ (mm)	D ₉₀ (mm)
Beach zone (1)	133.59	0.1949	0.3379	0.5905
Beach zone (2)	109.55	0.2098	0.3786	0.6235
Swash zone (3)	132.33	0.1598	0.3442	0.7180
Swash zone (4)	99.88	0.1651	0.3283	0.6243
Surf zone (5)	74.28	0.1247	0.3332	4.5630
Surf zone (6)	129.38	0.1296	0.3962	4.5761

Table 4. Sediment characteristics for the study area.

Table 4 reveals that the different zones have different sediment characteristics. The average grain size for the whole beach is assumed to be 0.3503 mm, fitting within the characteristics found by Wellmann (2014), as reported in chapter 2. The average grain sizes D₅₀ does not differ for the three zones and may be assumed as a constant throughout the beach. A clear separation is noticed in the D₉₀, i.e. the 90th percentile cumulative sediment value, which differs quite a lot for the beach/surf zone and the swash zone. This is explained through the presence of shells in the surf zone and in the sample.

5.5.2. Estimation of littoral transport rates

Returning to equations (3.11) and (3.12), an estimation of longshore sediment transport may now be given through the use of the CERC and Kamphuis-formulas, as stated below:

$$Q_{CERC} = \frac{K}{16(\rho_s - \rho)(1 - n)\sqrt{\gamma_b}} \rho \sqrt{g H_{sb}}^{5/2} \sin(2\theta_b) \quad (3.11)$$

$$Q_{Kamphuis} = 2.27 H_{sb}^2 T_p^{3/2} m_b^{3/4} D_{50}^{-1/4} \sin^{3/5}(2\theta_b) \quad (3.12)$$

A change may be noticed in the CERC-formula: instead of the usage of H_b, the significant wave height H_{sb} is used when describing total longshore transport. The Shore Protection Manual (USACE, 2001) is clear the two may be interchanged, and thus significant wave height is used.

Parameter	Value (dimension)	Remarks
ρ_s	2650 (kg/m ³)	Estimated from regular sediment density
ρ	1050 (kg/m ³)	Water density for salt water
n	0.32 (-)	Estimated for regular sediment characteristics with fine sand

γ_b	0.78 (-)	Estimated nearshore value by Wiggels (1972)
H_{sb}	0.2151 (m)	Average over the experiment period
θ_b	62.21 (-)	Average wave angle relative to coast over experiment period, converted using Snell's law and corrected for shallow water
T_p	1.87 (s)	Average over the experiment period
m_b	0.0497 (-)	Average beach slope for all profiles
D_{50}	0.0003503 (m)	See 5.5.1.
K	0.03 (-)	Assumed to be the same value as Medellin et al (personal comm.)

Table 5. Parameters and values used for longshore transport calculations.

Using the obtained parameters from the field data, the longshore transport rates can be calculated accordingly for the beachfront as a rate of sediment displacement per meter beach:

Method	Rate of displacement	Captured % by groin
CERC (USACE, 1966)	38.80 m ³ /day	46.4 %
Kamphuis (Kamphuis, 1991)	135.03 m ³ /day	13.3 %

Table 6. Longshore transport rates and captured percentage according to the Kamphuis and CERC formulas

Table 6 reveals the uncertainty in estimating longshore sediment transport. The CERC and Kamphuis formulas differ quite a lot, giving a disturbed image about the rate of longshore sediment transport. For both estimates, the groin is able to capture some percentage of the total volume displaced by the groin.

6. Discussion

6.1 Review of assumptions

During the course of this investigation, all measurements involving beach morphology were conducted using RTK survey based on GPS positioning in combination with height data. The measurements were conducted using a mobile rover mounted in a backpack. This backpack however caused some inaccuracies in the measurement. The actual position and height of the rover might not be exactly the same as the one of the observer, due to tilt in the backpack and extra added tilt of the rover due to walking. Data obtained by the Leica is therefore always some millimeters to some centimeters off in its determination of height and position next to the already incorporated error margin of 3mm when in connection with more than 5 satellites. Also, all points within the ‘accuracy margin’ of 50 cm around each transect do not reflect a true straight transect, and thus height measurements regarding these points are not per definition height measurements on the exact transect. Not only may the inaccuracies in height cause an issue regarding the beach profile. The setup of transects is also one of the parts causing error. The setup of the telescopic transect was assumed to be at all times perpendicular to the coastline. Due to the variable course of the coastline however, it was not always the case to have a perpendicular transect at every point.

Due to the inaccuracies in transects and height measurements, the estimated volume gain over all transects shows inaccuracies. The assumed interval over which volumetric integration was held is indeed correct for most transects directly around the groin, however it shows anomalies for the outermost transects due to issues with coastline position in the outermost transects, as explained in the both paragraphs above. Also, it is assumed that the beach profile shows the exact course of beach height over distance for the complete space around it. The beach profile in one transect reflects the beach profile as a whole for the space (2, 4, 5, 8, 10 or 15m around) separating them until encountering a new transect. All changes in between transects therefore were neglected and estimated as they were the same changes that happened in transect measured for the space considered. Volume calculation, especially for the far up- and downdrift sides is therefore not highly accurate and may be considered wrong. Volume gain at transects far up- and downdrift were not added in total volume gain, as they displayed no significant change under influence of the groin.

The bandwidth of natural variability was established for assessing if volume captured in transects fall within the range of natural variability. These natural changes, however, might be much larger than indicated by the bandwidth. The bandwidth was comprised of a mean of all volume gains and losses over a certain period of time. When assessing the volumes gained underneath transects, big volume gains may wrongly be associated as volume gains by a structure or another anomaly, causing a disturbance in the longshore sediment transport. Large pieces of beach are under constant movement of sediment, and even a slight anomaly in the natural composition of the bottom or a slight change in wind and wave patterns might alter the volume gain over the established transects. The bandwidth was intended as a tool to determine whether volumes gained by structural influence were significantly more than the average natural variability, and is used as a tool.

The determination of the rate of longshore sediment transport by the CERC and Kamphuis formulas present an order of magnitude differences. Mostly due to uncertainty in the parameters, of which for the CERC formula many were adopted from previous studies in the area, a high difference between the two can be witnessed. Uncertainty in empirically determined parameters like the K-value or the wave breaker index rely on a characteristic of the study area, and may be highly variable depending on the wave climate and sediment characteristics of a specific period. Especially the

estimate of the K-value, which is strongly dependent of the sediment characteristics of the area, is a factor of great uncertainty. In this estimate, the K-value was assumed to be the same as the experiment with the impermeable groin (Torres-Freyermuth, 2014). As stated before in chapter 3, the CERC-formula has the use of overestimating the rate of longshore sediment transport. Compared to previous studies involved with the use of the CERC-formula to estimate longshore transport of sediment (see Wang & Kraus, 1999), the K-value assumed for this study was significantly lower than those K-values used in that study. The lower K-value might explain why in this case, the CERC-formula had a lower prediction than the Kamphuis-formula.

6.2 Shoreline change: impermeable versus permeable groin (2)

In section 5.3, especially in figure 23, an overview of the shoreline change at an isobath of -0.3 m is given to give an indication about the shoreline changes of an impermeable groin versus a permeable groin. It was mainly done to show the similarity between coastline changes around an impermeable groin versus the permeable groin. These results, and other results like the volume gain and losses show the great similarity between the permeable groin used in the experiment and the impermeable groin used in a similar experiment.

This was an experiment with a specific kind of groin built up using different concrete elements. There are many more alternatives to permeable groins, for example wooden pilegroins, as described by Bakker et al. (1984). These wooden pilegroins are meant as an artificial hydraulic resistance in order to reduce longshore current velocity and reduce the rate of longshore sediment transport. It is in contrast to the groin used in the experiment, which relied on sediment trapping in order to reduce longshore current velocity and thus longshore sediment transport. It still allows for sediment to pass through, thus making it a semi-permeable groin. This semi-permeability seems to be confirmed by similarities in accretion and erosion patterns up- and downdrift of the groin. However, when looking at the downdrift patterns, the permeable groin seems to have a lesser impact compared to the impermeable groin. The erosion patterns on the downdrift side can also be explained by the fact that a degree of wave action to overtop the groin. The height of the groin was not enough to prevent wave action from reaching the downdrift side of the groin, thus causing wave action to reach the downdrift side. As the data is, it seems downdrift effects are reduced due to the permeability, but it is simply not known if in the long run, the semi permeable groin would display a similar pattern like the permeable groins.

Secondly, as the groin used in the experiment relied on partially trapping sediment, it decreased sediment budget on the downdrift side. The lessened sediment budget in the case of the experimental groin is still subject to some degree of erosion by overtopping waves and flow of water through the holes in the groin. Some degree of transport between the updrift and downdrift side by the water through the holes might occur, but it is not enough to balance out the sediment budget on the downdrift side. The only difference between the semi-permeable and impermeable groin is seen in the effect the both have far up- and downdrift, which is noticeably less for the semi-permeable groin.

Finally: does the permeable groin possess a quantitative or qualitative advantage over the use of the impermeable groin? Over the course of this experiment, it was found that the permeable groin offered a (potential) quantitative advantage over the impermeable groin. The volumetric gain by the impermeable groin was considerably less, but the results shows a connection between permeability and the reduced downdrift erosion in comparison to the application of an impermeable groin.

6.3 (Semi)-Permeable groin in erosion prevention

At this point, it is unknown if the design of the semi-permeable groin used in the experiment is suitable for long-term erosion prevention. During the 24h run, this specific design seemed to be a closer resemblance to an impermeable groin, indicating a usage on a larger scale might have the same downdrift effects as an impermeable groin. It would make the design much less useable for erosion prevention, as it only amplifies erosion problems downdrift. In order to work well, the design should be implemented as a groin field to reduce downdrift erosion.

The use of concrete elements proved to be reliable and resistant to wave action over the course of the field experiment. The elements in its current set-up at first moved slightly, but after 2h started digging in, providing an extremely stable structure. The concrete elements were heavy enough not to be lifted or extremely displaced by high-energy wave action and were found to be quite easily moveable and interlockable when setting up the groin for the experiment run. The use of concrete elements might therefore be a reliable and durable solution on the long run, as they are stable and need little maintenance to keep them in working order. Further research efforts should be devoted to analyse the impact of this type of structures on a longer time scale and stability during stormy conditions (e.g. Norte-events).

7. Conclusion and recommendations

7.1 Conclusion

The goal of this report was to investigate the impact of a permeable groin on longshore sediment transport and beach resilience on the beach in Sisal, Yucatán. It was done using a 24h experiment, in which continuous monitoring ensured the changes in beach morphology were monitored. These changes were monitored by using Real Time Kinematic surveys. Measurements regarding the natural circumstances were conducted by different measurement instruments measuring wave conditions, wind climate and tidal climate. After the 24h experiment, changes in beach morphology were surveyed to get an impression regarding beach resilience.

The natural variability of the beach in Sisal was found to be tied to sea-breeze events. Most importantly, a connection was found between wind speed and significant wave height with a correlation of 0.79, indicating a strong connection. From interpretation of the longshore sediment transport formulas of Kamphuis and the USACE/CERC it was discovered that the rate of longshore sediment transport was influenced via significant wave height to wind speed. The varying rate of longshore sediment transport with influences from cross-shore transport was found to be the reason behind the inter- and intra-day variability of bed levels along transects measured by RTK survey. An average natural bed level variability of - 0.09 m to 0.09 m was found valid for all transects and this bandwidth of natural bed variability was used to assess if bed levels along transects during the experiment period for the different transects eroded or accreted due to natural circumstances or structural influence.

During the 24h experiment, wave and wind conditions were found to be typical for sea-breeze events. Rate of bed level change varied during the day, with transects closely near the permeable groin showing volumetric gain at the updrift side and erosion at the downdrift side. However, bed level changes over the 24h were not constant, and displayed some degree of change during the day. It was explained by the occurrence undertow, over time causing more cross-shore transport, and wave transformation due to changes in bed level. In combination with the lowered current speed, it caused sediment transport decrease, explaining the smaller rate of accretion and erosion during calm periods without sea-breeze. Total volume gain over 24 hours was about 18 m³, with an updrift gain of 28.36 m³ and a downdrift erosion of 10.75 m³.

	Updrift (transect 3-10)	Downdrift (transect 11-19)
Volume gain (m ³)	28.36	- 10.75
Volume gain per m beach (m ³ /m)	0.59	- 0.23

Table 7. Volumetric gain updrift and downdrift of the permeable groin.

Shoreline change around the permeable groin resembled closely the typical pattern found for shoreline changes around an impermeable groin, with volume gain on the updrift side and volume loss found on the downdrift side. Far up- and downdrift sides were not found to be significantly changed. The impact of the permeable groin on the beach over 24h is significantly less, expressed in the total volume gain of 18 m³ for the permeable groin and 60 m³ for the impermeable groin. However, due to the running time of the experimental setup, it is simply unknown if the shoreline characteristics of a permeable groin would display a similar pattern as an impermeable groin over a longer running time.

Beach resilience of the Sisal beach was found to be strong. After 4 hours, the first signs of recovery were found on the updrift side, whilst on the downdrift side slight erosion occurred due to the

influence of the sea-breeze events. Within 24h, the beach completely recovered from the influence of the groin.

At this point, it is unknown if the design of the permeable groin used in the experiment is suitable for long-term erosion prevention. During the 24h run, this specific design seemed to be a closer resemblance to an impermeable groin, indicating a usage on a larger scale might have the same downdrift effects as an impermeable groin. It would make the design much less useable for erosion prevention, as it only amplifies erosion problems downdrift.

7.2 Recommendations

For follow-up research regarding the impact of (semi)-permeable groins on longshore sediment transport, it is recommended to research the impact of different degrees of permeability on longshore sediment transport. The semi-permeable groin used in this specific experiment had a low rate of permeability, and comparing its results to a true permeable groin would give a better idea of the impact of a true permeable groin on beach morphology.

Secondly, the interaction between up- and downdrift sides by flow of sediment deserves more attention. During the course of the experiment, it was clear that due to permeability, a degree of sediment moves from the updrift side to the downdrift side through the holes in the groin. This sediment displacement shows when closely examining the shoreline change, but it is not known how this flow of sediment interacts with permeability.

Finally, running time of the experiment should be increased for a next investigation to be able to observe the shoreline change during a longer period of time. A 24 hour investigation is long enough to witness initial changes in the shoreline, but it does not cover shoreline change during a longer period of time. Also, a permeable structure over a longer period of time might display different shoreline characteristics due to its permeable points filling up with sediment. Therefore, more research should be conducted in the shoreline change around (semi)-permeable groins over a longer period of time.

8. References

- Appendini, C.M., Salles, P., Mendoza, E.T., López, J. and Torres-Freyermuth, A., 2012. "Longshore Sediment Transport on the Northern Coast of the Yucatan Peninsula". *Journal of Coastal Research*, 28(6), Coconut Creek (Florida), p. 1404-1417.
- Bakker, W.T., Hulsbergen, C.H., Roelse, P., De Smit, C. And Svasek, J.N. (1984). "Permeable Groynes: Experiments and Practice in the Netherlands." *Coastal Engineering Proceedings*, 1(19), 1984.
- Brown, J., Colling, A., Park, D., Rothery, D. and Wright, J. (1989). "Waves, Tides and Shallow-Water Processes". *Open University*.
- CINVESTAV, 2007. Programa de Ordenamiento Ecológico del Territorio Costero del Estado de Yucatán (POETCY). Mérida, México, Centro de Investigación y de Estudios Avanzados del IPN, Unidad Mérida (CINVESTAV).
- Coastal Engineering Research Center, 1966, 1984, 2001. "Shore protection manual". CERC, department of the Army, Waterways Experiment Station, United States Army Corps of Engineers Vol. 1, Vicksburg MS.
- Cuevas-Jiménez, A., Euán-Ávila, J. (2009). "Morphodynamics of carbonate beaches in the Yucatán Peninsula". *Ciencias Marinas*, 35, p. 307-320
- Enriquez, C., Mariño-Tapia, I., Herrera-Silveira, J. (2010). "Dispersion in the Yucatán Coastal zone: Implications for Red Tide Events". *Continental Shelf Research*, 30 (2), p. 127-137.
- Galvin, C. (1979). "Relation between immersed weight and volume rate of longshore transport". CERC TP 79-1, Coastal Engineering Research Center, Washington D.C. 15pp.
- Güner, H., Yüksel, Y., Cevik, E. (2011). "Determination of Longshore Sediment Transport and Modelling of Shoreline Change". *Sediment Transport*, (2), p. 117-136.
- Hanson, H., Kraus, N.C. (1991). "GENESIS: Generalized Model for Simulation Shoreline Change". CERC Report 89-19, Reprint, U.S. Army Corps of Engineers (USACE), Vicksburg.
- Hoefel, F. and Elgar, S. (2003). "Wave-induced sediment transport and sandbar migration." *Science* 299(5614), p. 1885-1887.
- Lira-Pantoja, M.A., Torres Freyermuth, A., Appendini, C.M., Fernández, D., Salles, P. Mendoza, E.T., López and J. Pedrozo-Acuña, A. (2012). "Chronic Beach Erosion Induced by Coastal Structures in Chelem, Yucatán." *Coastal Engineering Proceedings*, 1(33), 125.
- Longuet-Higgins, M.S. (1970). "Longshore currents generated by obliquely incident sea waves: 1." *Journal of Geophysical Research* 75.33 (1970): 6778-6789.
- Kamphuis, J. (1991). "Alongshore Sediment Transport Rate". *Journal of Waterway, Port, Coastal and Ocean Engineering*, 10.1061/(ASCE)0733-950X(1991), 117:6(624), p. 624-640.
- Kraus, N.C., Hanson, H. and Blomgren, S.H. (1994). "Modern Functional Design of Groin Systems." *Coastal Engineering Proceedings*, 1(24)
- Medellín, G., Mariño-Tapia, I., and Euán-Ávila, J. (2015). "The Influence of a Seawall on Postnourishment Evolution in a Sea-Breeze Dominated Microtidal Beach". *Journal of Coastal Research*, 31(6), Coconut Creek (Florida), p. 1449-1458.

- Meyer-Arendt, K.J. (1991). "Tourism Development on the North Yucatan Coast: Human Response to Shoreline Erosion and Hurricanes". *GeoJournal* 23.4 (1991), p. 327-336.
- Meyer-Arendt, K.J. (2001). "Recreational development and shoreline modification along the north coast of Yucatán, Mexico". *Tourism Geographies*, 3(1), p. 87-104.
- Nortek A.S. (2001). "Vector User Manual ver. D", Nortek A.S. c.2001, pub. No. N300-100.
- Otay, E.N., Güngörđü, Ö. and Börekçi, O.S. (1997). "Shoreline Changes in the Vicinity of a Permeable Groin". *Coastal Engineering Workshop*, Istanbul, Turkey.
- Ribberink, J. (n.d.). "Marine Dynamics". University of Twente, 2016.
- Scott, T., Masselink, G. and Russell, P. (2011). "Morphodynamic characteristics and classification of beaches in England and Wales." *Marine Geology* 286.1 (2011): p. 1-20.
- Sharpe, M.M. (1990). "The distribution of wave heights and periods for seas with unimodal and bimodal power density spectra." *Woods Hole Oceanographic Institution*, Massachusetts Institute of Technology, 1990.
- Soler-Bientz, R., Watson, S., Infield, D. (2010). "Wind Characteristics on the Yucatán Peninsula based on short-term data from meteorological stations." *Energy Conservation and Management* 51 (2010), p. 754 - 764.
- Teledyne RD Instruments (2011). "Acoustic Doppler Current Profiler Principles of Operation: a Practical Primer." P/N 951-6069-00 (January 2011).
- Torres-Freyermuth, A., Puleo, J.A., Ruiz de Alegría-Arzaburu, A., Figlus, J. (2014). "Nearshore Coastal Dynamics on a Sea-Breeze Dominated Micro-Tidal Beach (NCSAL)." *American Geographical Union conference paper*, 2014, San Francisco.
- Uc-Sánchez, E. (2009). "Efectos de los Cambios de la Playa, sobre los Hábitats Bentónicos en el Puerto de Progreso, Yucatán". *Conkal, Mexico: Instituto Tecnológico de Conkal*, 72p.
- Van der Velden, E.T.J.M. (1989). *Coastal Engineering*. (2), TU Delft.
- Voulgaris, G. And Trowbridge, J.H. (1998). "Evaluation of the Acoustic Doppler Velocimeter (ADV) for Turbulence Measurements", *Journal of Atmosphere and Ocean Technology*, 15 (1998), p. 272-289.
- Wang, P., Kraus, N.C. (1999). "Longshore Sediment Transport Rate Measured by Short-Term Impoundment". *J. Waterway, Port, Coastal, Ocean Eng.*, 10.1061/ (ASCE) 0733-950X (1999) 125:3 (118), p. 118-126.
- Wellman, N. (2014). "Analysis of Near-Shore Sediment Samples from Sisal Beach (Mexico) and comparing effect of Sea Breeze and El Norte Events." *HWTK Leipzig*, 2014.
- University of California, Santa Barbara (2016). "UCSB Beach: 45 years of Waxing and Waning." *Images retrieved at 28-6-2016 at http://www.geol.ucsb.edu/faculty/sylvester/UCSB_Beaches /UCSBbeaches .html*
- Weggel, J.R. (1972). "Maximum Breaker Height for Design". *Coastal Engineering Proceedings* 1.13 (1972).

Appendix A. Overview of used instruments

In chapter 4, a brief description is given of the principles of Real Time Kinematic (RTK) survey technique and the Doppler velocimetry technique. However, since this overview is not very detailed, the basic principles of RTK and ADV will be explained into detail here. Next, the precise use of the LEICA GS14/CS15 GNSS and the Nortek VECTOR are explained in more detail.

Principles of RTK survey

The Real Time Kinematic (RTK) survey technique is a technique used to derive and enhance the precision of position data derived from global navigation satellite systems (GNSS) such as GPS, GLONASS, Galileo and GAGAN and was developed in the 1990's. Predominantly, it uses measurements of the phase of the signal's carrier wave, rather than the information or content stored in the signal, and a reference station or virtual station to determine position of a mobile receiving device, or rover, to send real-time corrections of position, allowing for centimeter- to millimeter accuracy.

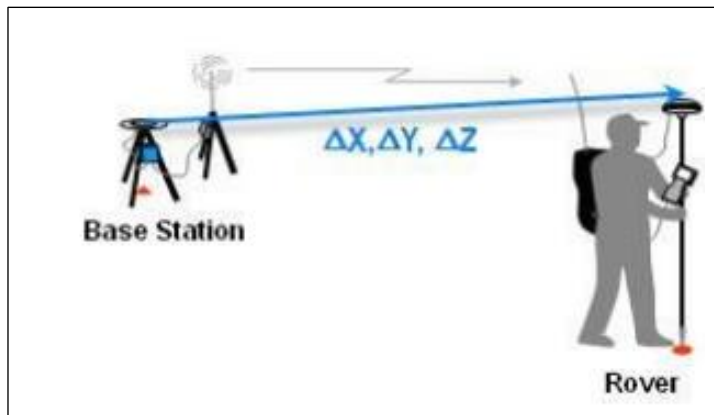


Figure 29. Overview of RTK position and setup.

From a point of view, as can be seen in figure 29, the total setup using RTK consists of a base receiver, one or more mobile rovers, and a radio which enables the use of a communications channel to send correction data in real time to the user.

RTK is used to measure both the position of the base and the rover relative to each other. The basic principle is the difference in phase of the carrier wave between the base

and the rover. Both the rover and the base use the same constellation of satellites. Using their carrier waves while ignoring the information stored within the signal, both the base and the rover establish their position relative to the position of the satellite, measured in wavelengths. The base station, which is on a known position, transmits its raw observations of its received GPS position via an UHF radio connection to the rover in real time. With the correction data sent by the base station, the rover uses both the base station data and its own obtained data to determine its position on an x-y-z-plane relative to the base in real time.

RTK yields a positional accuracy from 2 cm up to 5 mm for determining position. Errors however may occur in measurements, and are mostly due to a number of circumstances regarding the principle:

- Distance between the rover and base station: up until 20 km from the base point, RTK yields a precise determination of position. Longer distances may cause error, mostly due to the correction information, sent to the rover using a regular radio (UHF-) connection. UHF signals only have a strong signal range up to 20 km (or 30 kms when clear weather).
- Errors in reception of GNSS or UHF signals: when surveying, RTK requires a reliable connection between the base and the rover, because the rover needs continuous information from the base to determine its position. A disturbance in GNSS data sent to the base from satellites or a disturbance in UHF signals may cause the rover to lose signal.

- Number of satellite signals received: in order to determine the exact position of the base and the rover, it is essential to have multiple satellite locks. Each satellite has a certain bias regarding global positioning. The bias becomes significantly less when using multiple satellites to determine position, due to their biases canceling each other out. In order to receive a good position lock, at least 5 satellites should be locked on to the position.

Most of the errors described above yield an error for both the base and the rover. However, since the errors are constant for both the base and the rover (they receive the exact same signal), these errors cancel each other out. Therefore, the relative distance between the rover and the base, in combination with the quality of the received signal from the satellites is the determining factor in positional accuracy. When having the right L2 signal from satellites and staying within 10 km of the base, positional accuracy is most often around 2 mm.

Use of LEICA GS14/CS15 GNSS total system



Figure 30. RTK equipment used to measure transect change.

The LEICA GS14 GNSS Smart Antenna (1) and LEICA Viva CS15 Controller (2) are instruments commonly used in RTK survey. The system consists of two GS14 Smart Antennas, to be used as base station, or to be used as rover, and the Viva CS15 Controller, for OTF measurement display of the measurements by the rover. The LEICA systems are used in combination with a Satel SATELLINE-EASY pro IP67 35W UHF (3) radio on a dedicated channel for transmission of the correction data from the base to the rover. The equipment is visible in figure 30.

One of the two Leica GNSS receivers (1) is used in combination with the Satel radio (3) to be used as a base and a transmission radio to send a correctional UHF signal to the second GNSS receiver (1). This second GNSS receiver is used as the mobile rover in the backpack (4) at the back of the observer, and is in direct connection with the controller (2), on which real time position can be monitored. The controller stores all the data received from the rover (1) and makes it accessible to view at any moment. The output of the controller is a specific Leica format, which with coordinate systems can be converted to a simple .txt-file. The .txt file consists of all the coordinates received

on the data points along transects, revealing the measured X and Y coordinate of a datapoint, together with the measured height relative to the base and relative to the local measured zero sea level.

Principles of acoustic Doppler velocimetry (ADV)

The acoustic Doppler velocimetry (ADV) technique is a widely used technique designed for obtaining and recording velocity components in a flow with a small sample volume with a high frequency (Voulgaris and Trowbridge, 1998).

The basic principle behind the measurements is the measurement of particles in a flow volume using the Doppler Effect for shifting objects. A simple example can be given in order to illustrate the working of the Doppler Effect. When standing next to a road and noticing a car blowing its horn, it has a certain frequency. However, when the car moves by, a change in tone is noticed. This is caused by the compression of sound waves in front of a moving vehicle (thus a higher frequency) and the relaxation of sound wave compression behind the car (thus a lower frequency). The shift in frequency therefore may be described as:

$$F_{doppler} = F_{source} \frac{V}{C}$$

With $F_{doppler}$ as the change in frequency (Doppler shift), F_{source} as the frequency of transmitted sound by the source, V as the speed of the moving source relative to the observer and C as the speed of sound.

The Nortek Vector Acoustic Doppler Velocimeter

Information about the workings of the ADV is taken from the “Vector Current Meter User manual”, written by Nortek AS. (2005).

Sampling rate	16 Hz
Burst interval	Continuous measurement/no bursts
Sampling volume	14.9 mm ³
Head frequency	6000 kHz
Coordinate system	XYZ

Table 8. Vector ADV setup parameters during the course of the experiment.

The same principle is used by the ADV to measure water velocity in three velocity components. The system has three main components: acoustic sensor, consisting of a transmitter and three or more receivers, a conditioning module and a processing module, visible in figure 31. The acoustic sensor is mounted at the end of a thin rod (stem) to minimize influence on the flow. While measuring, the

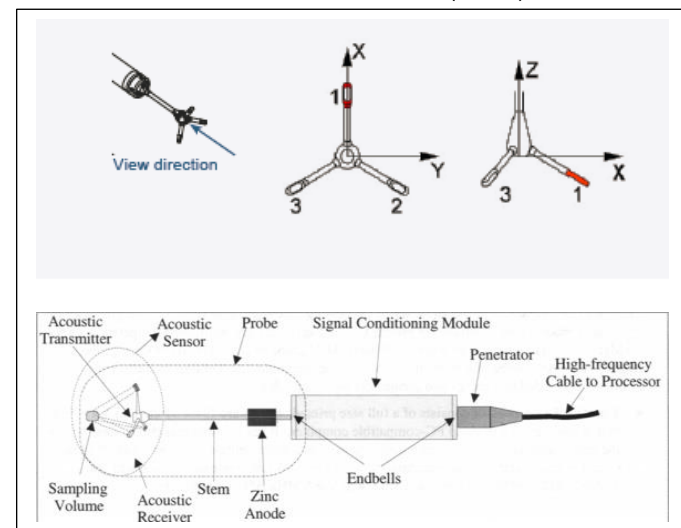


Figure 31. Vector head and axis (a), and components of the Nortek Vector (b).

acoustic probe sends out short acoustic pulses on a fixed frequency along a transmit beam. The three transducers (receivers) are all focused on a small control volume and pick up a fraction of the acoustic pulses by ‘listening’ to the change in frequency. These pulses are reflected back by small particles in the control volume. Because the particles move at the same speed as the water that carries them, the current speed may be determined by the Doppler shift. The three receivers pick up the echoes originating from the control volume and process the Doppler shift by the particles with respect to each transducer. The

Nortek Vector ADV besides having the acoustic transmitter, is also equipped with a pressure sensor to measure its depth relative to the sea surface. All measurements are directly sent to a processor module for processing and storage of data.

Different wave parameters can be obtained from the data of the Vector. Wave height may be obtained by the Z-direction of the transducer information. Current speed and current direction is obtained from the X and Y-direction of the transducer data while tidal information may be obtained from the pressure sensor. Data is conveniently outputted in different files for the Vector. The data of the different sensors onboard of the Vector output its files in a sensors data file (.sen), a burst header data file containing all noise and error checks (.vhd), velocity data file (.dat) with all velocities measured, and a header file (.hdr) to explain how every file is built up and with all checks of important instruments.

The RD Instruments WorkHorse Acoustic Doppler Current Profiler (ADCP)

Information of the workings of the ADCP is taken from “Acoustic Doppler Current Profiler: Principles of Operation”, written by Teledyne RD Instruments (2011).

Contrary to the Nortek Vector ADV, the RD instruments ADCP, visible in figure 32, is a 3D current profiler, not being able to do high precision wave measurements, but is purely intended for current



Figure 32. An RD Instruments ADCP.

profiling. Most importantly, they can measure velocity profiles over different depths. Like the ADV, the ADCP uses pulses to measure velocity of water. However, in contrast to the ADV, which is focused on a small portion of volume, the ADCP is focused on a complete depth profile, often being able to measure large water columns directly above the ADCP.

Velocity is measured through the four big transducers on top of the ADCP (the red patches). Velocity is measured on the principle of time dilatation: like the ADV, it measures a volume of water using sound pulses and the Doppler shift. However, the ADCP focuses on the time traveled by the pulses to determine the location of particles in the water. A change in travel time corresponds to a change of distance per pulse. Knowing the change in travel time and the speed of sound in water, the velocity of a particle can be measured at a certain depth. The assumption made here is that the particles in the water move at the same speed as the current speed.

The transducer beams are set up in a ‘Janus’ configuration, being able to see in four different directions. The four pair of beams pick up velocities in pairs: one set of beams obtains the horizontal and vertical velocity component in a north-south setup, the second pair of beams obtains at the same time a second horizontal and vertical velocity component. The horizontal velocity is used to compute current velocity and direction, while vertical velocity is used to compute a current speed profile and most importantly wave height. Data is very simply outputted in a post-processed file containing current velocity, current speed, current direction and wave height.